

1 **Title:** Unconventional secretion of unglycosylated ORF8 is critical for the cytokine
2 storm during SARS-CoV-2 infection
3 **Running Title:** Life Finds a Way: the unconventional secretion of ORF8
4 **Authors:** Xiaoyuan Lin^{1, #}, Beibei Fu^{1, #}, Yan Xiong¹, Na Xing², Weiwei Xue³, Dong
5 Guo¹, Mohamed Y. Zaky⁴, Krishna Chaitanya Pavani⁵, Dusan Kunec², Jakob
6 Trimpert² and Haibo Wu^{1, *}
7 ¹School of Life Sciences, Chongqing University, Chongqing 401331, China
8 ²Institute of Virology, Free University of Berlin, Berlin 14163, Germany
9 ³School of Pharmaceutical Sciences, Chongqing University, Chongqing 401331,
10 China
11 ⁴Molecular Physiology Division, Faculty of Science, Beni-Suef University, Beni-Suef,
12 Egypt
13 ⁵Department of Reproduction, Obstetrics and Herd Health, Ghent University, B-9820
14 Merelbeke, Belgium
15
16 [#]These authors contributed equally to this work
17 ^{*}**Corresponding author:** Haibo Wu, School of Life Sciences, Chongqing University,
18 Chongqing 401331, China; E-mail: hbwu023@cqu.edu.cn
19
20
21
22

23 **Abstract**

24 Coronavirus disease 2019 is a respiratory infectious disease caused by the severe
25 acute respiratory syndrome coronavirus 2 (SARS-CoV-2). Evidence on the
26 pathogenesis of SARS-CoV-2 is accumulating rapidly. In addition to structural
27 proteins such as Spike and Envelope, the functional roles of non-structural and
28 accessory proteins in regulating viral life cycle and host immune responses remain to
29 be understood. Here, we show that open reading frame 8 (ORF8) acts as messenger
30 for inter-cellular communication between alveolar epithelial cells and macrophages
31 during SARS-CoV-2 infection. Mechanistically, ORF8 is a secretory protein that can
32 be secreted by infected epithelial cells via both conventional and unconventional
33 secretory pathways. The unconventionally secreted ORF8 recognizes the IL17RA
34 receptor of macrophages and induces cytokine release. However, conventionally
35 secreted ORF8 cannot bind to IL17RA due to N-linked glycosylation. Furthermore,
36 we found that Yip1 interacting factor homolog B (YIF1B) is a channel protein that
37 translocates unglycosylated ORF8 into vesicles for unconventional secretion.
38 Blocking the unconventional secretion of ORF8 via a YIF1B knockout in hACE2
39 mice attenuates inflammation and yields delayed mortality following SARS-CoV-2
40 challenge.

41

42 **Keywords:** SARS-CoV-2, Secretory protein, Unconventional secretory pathway,
43 Glycosylation, YIF1B

44

45 **Introduction**

46 Coronavirus disease 2019 (COVID-19), caused by severe acute respiratory syndrome
47 coronavirus 2 (SARS-CoV-2), is continuing to spread around the world with nearly
48 256 million confirmed cases and more than 5.1 million deaths. According to clinical
49 case reports, critically ill patients with COVID-19 experience a cytokine storm,
50 resulting in acute respiratory distress syndrome and multiple organ failure(1, 2).
51 Currently, our understanding of the mechanisms behind the cytokine storm and how
52 SARS-CoV-2 affects cytokine release is still limited.

53

54 Open reading frame 8 (ORF8) is an accessory protein of SARS-CoV-2 and it is one of
55 the most rapidly evolving β -coronaviruses proteins(3). A 29 nucleotide deletion in
56 ORF8 is the most obvious genetic change in severe acute respiratory syndrome
57 coronavirus (SARS or SARS-CoV-1) during its host-jump from bats to humans(4).
58 The $\Delta 382$ variant of SARS-CoV-2, which eliminates ORF8 transcription, seems to be
59 associated with milder infection and less systemic release of pro-inflammatory
60 cytokines(5). In a previous study, we demonstrated that ORF8 contributes to the
61 cytokine storm during SARS-CoV-2 infection(6). Specifically, we found ORF8 to
62 interact with the IL17RA receptor, leading to excessive activation of IL-17 signaling
63 and downstream NF- κ B pathway. However, it remains unclear how the virus exposes
64 ORF8 to enable access to the extracellular domain of IL17RA.

65

66 In eukaryotes, secretory proteins usually contain a signal peptide that triggers

67 translocation into the endoplasmic reticulum (ER)(7). Following this translocation to
68 the ER, cargoes will be exported through ER-Golgi trafficking for further processing
69 and modification(8, 9). This process is termed conventional secretion. Besides, many
70 cytosolic proteins without signal peptides, such as fibroblast growth factor 2 and yeast
71 Acb1, can be released through an unconventional protein secretion pathway(10, 11).
72 Recently, Zhang et al. identified TMED10 as a protein channel for vesicle entry and
73 secretion of interleukin 1 family members(12). Evidently, viral proteins can hijack this
74 secretion pathway to become secreted. For example, the HIV-1 Nef protein can be
75 released from infected cells via an exosomal pathway(13, 14). However, very little is
76 known about whether and how SARS-CoV-2 encoded proteins are secreted during
77 infection.

78

79 Glycosylation is a common posttranslational modification, it involves the addition of
80 glycans to macromolecules and is considered essential for the correct folding and
81 functional performance of proteins(15-17). It is also not uncommon for proteins from
82 pathogens to be glycosylated by the host. The co-evolution of N-linked glycosylation
83 sites in influenza viruses affects the host specificity(18). The glycosylation of viral
84 envelope proteins has a wide range of functions, including regulating cell tropism,
85 protein stability and immune evasion(19-21). Recent studies have shown that
86 SARS-CoV-2 Spike protein has 22 N-linked glycosylation sites and 17 O-linked
87 glycosylation sites, which may influence viral infectivity and pathogenicity(22-24). In
88 contrast to the situation for the Spike protein, glycosylation and its functional role in

89 accessory proteins of SARS-CoV-2 has not yet been reported.

90

91 Here, we identified SARS-CoV-2 ORF8 as a secretory protein that can be secreted via
92 conventional and unconventional secretory pathways at the same time. We found that
93 unglycosylated ORF8 secreted via an unconventional pathway is responsible for the
94 release of pro-inflammatory cytokines by binding the IL17RA receptor. By contrast,
95 conventionally secreted ORF8 is incapable of binding to IL17RA due to the N-linked
96 glycosylation at Asn78 site. Further, we identified Yip1 interacting factor homolog B
97 (YIF1B) as a channel protein that recognizes and translocates unglycosylated ORF8
98 into vesicles, thus enabling unconventional secretion. Our findings present an
99 important contribution to the understanding of how SARS-CoV-2 promotes the onset
100 of cytokine storm, and provide a promising strategy for the development of
101 COVID-19 therapeutics.

102

103

104 **Results**

105 **SARS-CoV-2 ORF8 is a secretory protein that is associated with cytokine release**
106 In order to investigate the secretion of ORF8 protein, we infected Calu-3 human lung
107 epithelial cells with SARS-CoV-2 that was generated using a reverse genetic system
108 (25-27)(Fig. 1A). Cell culture supernatant was collected and presence of ORF8 was
109 determined by ELISA and western blotting (Fig. 1B). We found that ORF8 protein
110 can be secreted into cell culture medium (Fig. 1C). To further validate these results,

111 we used the non-secretory SARS-CoV-2 main proteinase (M pro, also known as 3CL
112 pro) non-secreted control, and the well-known Nef secretory protein of HIV-1 (13, 14)
113 as a secreted protein control. We found that Jurkat cells secreted Nef protein
114 following HIV-1 infection, and Calu-3 cells secreted ORF8 protein after being
115 infected with SARS-CoV-2 (Fig. 1D). By contrast, the structural protein 3CL pro was
116 not secreted (Fig. 1D). Next, we tested the time-dependency of ORF8 secretion in
117 Calu-3 epithelial cells. After 12 hours of SARS-CoV-2 infection, the cell culture
118 medium was replaced and ORF8 protein in the supernatant was detected every 2
119 hours. Using 3CL pro as a negative control, we found that the secretion of ORF8
120 continued for at least 12 hours after replacing the culture medium (Fig. 1E). These
121 results indicated that SARS-CoV-2 ORF8 is a secretory protein.

122

123 Our previous study has shown that ORF8 protein contributes to the cytokine storm
124 during SARS-CoV-2 infection(6). SARS-CoV-2 mainly invades alveolar epithelial
125 cells through binding to ACE2 receptors, however monocytes/macrophages play a
126 critical role in the secretion and regulation of cytokines. Next, we generated a
127 SARS-CoV-2 variant with an ORF8 deletion (Fig. 1F), and constructed an epithelial
128 cell-macrophage co-culture system using a Transwell setup (Fig. 1F), to answer the
129 question that whether ORF8 is a key factor in modulating the transmission process of
130 infection signals from epithelial cells to monocytes/macrophages. In this system, the
131 release of pro-inflammatory factors in macrophages infected with either wild-type
132 SARS-CoV-2 or ORF8-deletion variant was increased, probably due to a small

133 amount of ACE2 receptor expressed on the surface of macrophages (Fig. 1G, H).

134 Interestingly, we found that the amount of pro-inflammatory factors in the co-culture

135 system was much higher than that measured in individual epithelial cells or

136 macrophages infected with wild-type SARS-CoV-2 (Fig. 1G). However, this

137 synergistic pro-inflammatory effect between epithelial cells and macrophages was not

138 observed in the ORF8-deletion virus infected group (Fig. 1H). Considering that ACE2

139 is responsible for virus entry(28, 29), and IL17RA is the receptor of ORF8(6), we

140 generated ACE2-deficient epithelial cells (Calu-3 *Ace2*^{-/-}) based on Calu-3 cell line,

141 and IL17RA-deficient macrophages [THP-1-derived macrophages (THP-1 DM)

142 *Il17ra*^{-/-}] based on THP-1 cell line (Fig. S1A). By using these two ways to disrupt

143 cellular communication between epithelial cells and macrophages, preventing

144 SARS-CoV-2 entry by ACE2 deletion in Calu-3 *Ace2*^{-/-} cells, or interrupting ORF8

145 reception by IL17RA deletion in THP-1 DM *Il17ra*^{-/-} cells, a significant

146 downregulation of pro-inflammatory factors was observed in the co-culture system

147 (Fig. 1H). These results implied that inter-cellular communication between epithelial

148 cells and monocytes/macrophages is important for the cytokine release during

149 SARS-CoV-2 infection.

150

151 It is known that secretory proteins, such as Nef, can be secreted in absence of viral

152 infection in an *in vitro* system(13). We therefore tested whether ORF8 protein can be

153 secreted by human embryonic kidney (HEK-293FT) cells transfected with an

154 ORF8-Flag plasmid. The results showed that Flag-tagged ORF8 was secreted in

155 absence of SARS-CoV-2 infection (Fig. S1B, C). Furthermore, the supernatant of
156 cells transfected with ORF8-Flag was collected and added to the culture medium of
157 THP-1 DM cells for stimulation. In this setup, the release of pro-inflammatory factors
158 in THP-1 DM cells stimulated with ORF8-Flag transfection supernatant was
159 significantly increased compared to cells treated with control supernatant (Fig. S1D).
160 In summary, we demonstrated that SARS-CoV-2 ORF8 is a secretory protein, and that
161 extracellular ORF8 protein is of greatly promoting cytokine release.

162

163 **SARS-CoV-2 ORF8 has an unconventional secretory pathway**

164 In order to understand the secretion pattern of ORF8, we used an online tool, Simple
165 Modular Architecture Research Tool (SMART, <http://smart.embl-heidelberg.de>), to
166 analyze structural domains of the ORF8 protein. We found a hydrophobic central
167 domain (similar to the conserved signal peptide of eukaryotes) to be located at its
168 N-terminus. We defined this domain as the signal peptide of ORF8 protein. Signal
169 peptide-deficient mutant (Δ Signal-SARS-CoV-2 ORF8) was constructed and
170 transfected into Calu-3 epithelial cells and HEK-293FT cells, respectively (Fig. 2A).
171 The result showed that the secretion ability of ORF8 was substantially impaired by
172 signal peptide deletion (Fig. 2B, C). Interestingly, an appreciable quantity of signal
173 peptide-deficient ORF8 was observed in both the supernatant of Calu-3 and
174 HEK-293FT cells. This result strongly suggested that the secretion of ORF8 is not
175 completely blocked by the signal peptide deletion (Fig. 2B, C). This data implied that
176 secretion of ORF8 might not completely depend on the presence of the signal peptide.

177

178 Proteins secreted through the conventional secretory pathway contain an N-terminal
179 signal peptide, which is recognized by the signal recognition particles and transported
180 into the ER, followed by signal peptide cleavage and trafficking to the Golgi
181 apparatus and the subsequent endomembrane system(7). To verify the existence of an
182 unconventional secretory pathway for ORF8, Brefeldin A(30) or Monensin(31) was
183 used to inhibit the Golgi-related vesicle transportation. Consistent with our previous
184 result, secretion of ORF8 was still observed when the conventional secretory pathway
185 was blocked (Fig. 2D, E).

186

187 To understand whether the secretion pattern of ORF8 is evolutionary conserved, we
188 analyzed the homologous ORF8 of SARS and found the SARS ORF8a isoform to
189 contain an N-terminal signal peptide. We then constructed a ΔSignal-SARS ORF8a
190 mutant and transfected it into epithelial cells (Fig. 2F). While the intact SARS ORF8a
191 was secreted normally (Fig. 2G), the ΔSignal-SARS ORF8a lost the secretory ability
192 completely (Fig. 2G). This finding stands in interesting contrast to our results showing
193 that SARS-CoV-2 ORF8 is secreted in absence of the signal peptide (Fig. 2G). This
194 finding was further supported by inhibition of the Golgi-related vesicle transport
195 using Brefeldin A or Monensin in Calu-3 (Fig. 2H) and HEK-293FT cells (Fig. 2I).
196 The results obtained here show that SARS ORF8a can only be secreted under the
197 guidance of signal peptide through the conventional secretory pathway.

198

199 Considering that the signal peptides of these two different ORF8 proteins share
200 distinct sequences, we asked whether the different secretion patterns of ORF8 is due
201 to the different types of signal peptide. To examine this hypothesis, we exchanged the
202 ORF8 signal peptides between SARS and SARS-CoV-2 (Fig. 2J). As a result,
203 exchange of signal peptides did not change the secretory patterns observed for the two
204 viruses (Fig. 2K). Specifically, SARS-CoV-2 ORF8 carrying the SARS ORF8a signal
205 peptide was still secreted when the Golgi-dependent secretory pathway was blocked
206 (Fig. 2K). Taken together, these results indicated that SARS-CoV-2 ORF8 is likely to
207 have an unconventional secretion pattern that does not depend on the presence of a
208 signal peptide.

209

210 **Unconventional secretion of ORF8 is required for cytokine storm**

211 Next, we studied whether the different secretion patterns of ORF8 are associated with
212 the release of pro-inflammatory factors. Calu-3 epithelial cells were pretreated with
213 Brefeldin A or Monensin to block the conventional secretory pathway, then cells were
214 infected with SARS-CoV-2 and culture supernatant was collected to stimulate THP-1
215 DM cells. After 12 hours, pro-inflammatory factors secreted by macrophages were
216 examined by ELISA (Fig. 3A). Surprisingly, although the amount of secreted ORF8
217 was significantly decreased (Fig. 3B), the release of pro-inflammatory factors was
218 barely affected by Brefeldin A or Monensin treatment (Fig. 3C). In order to rule out
219 the possibility of mutual influence between macrophages themselves, we tested
220 pro-inflammatory factors released by THP-1 DM cells stimulated with supernatant at

221 different time intervals. The result showed that there were no significant differences in
222 the secretion of pro-inflammatory factors by macrophages within 0-12 h (Fig. 3C, Fig.
223 S2A). Further, we used exogenously expressed Flag-tagged ORF8 (Fig. 3A), instead
224 of SARS-CoV-2 virus, to validate this finding. Consistent with previous results, we
225 observed almost equal expression levels of pro-inflammatory factors induced by
226 ORF8-Flag regardless of the Golgi-dependent secretory pathway blockade (Fig. 3D,
227 Fig. S2B). These results implied that the unconventionally, instead of the
228 conventionally secreted ORF8 is responsible for the cytokines release.

229

230 The current data point to a potential possibility that ORF8 secreted via different
231 pathways might undertake different responsibilities. Interestingly, in our western blots,
232 a smear band shifted to a higher molecular mass compared to ORF8 was regularly
233 observed, this smear however disappeared when the conventional secretory pathway
234 was inhibited by signal peptide deletion or Golgi apparatus damage (Fig. 2B, D, E).

235 Increasing the acrylamide concentration of the SDS-PAGE gel and prolonging the
236 electrophoresis time, we were finally able to distinguish a second band of secreted
237 SARS-CoV-2 ORF8 (Fig. 3E). The Golgi apparatus is known to be the workshop for
238 protein trafficking and processing(32), the most common form of protein processing
239 in Golgi apparatus is glycosylation(16). With this in mind, we asked whether ORF8 is
240 glycosylated during the conventional secretory pathway, which might be responsible
241 for the band shift. Using PNGase F or O-Glycosidase + α 2-3, 6, 8, 9 Neuraminidase A,
242 we tested the glycosylation status of ORF8 protein secreted from Calu-3 cells infected

243 with SARS-CoV-2. We found that PNGase F treatment, which hydrolyzes most of the
244 N-linked glycans(33, 34), was leading to the formation of a single ORF8 protein band
245 (Fig. 3E). Digesting SARS-CoV-2 ORF8 with O-linked glycan hydrolase
246 O-Glycosidase and α 2-3, 6, 8, 9 Neuraminidase A did not change the type of bands
247 compared to untreated samples (Fig. 3E). These data suggested that part of the
248 secreted SARS-CoV-2 ORF8 protein was N-glycosylated, and that this is likely a
249 result of conventional secretion through the Golgi apparatus. By contrast, SARS
250 ORF8a did not respond to glycoside hydrolases at all (Fig. S2C), which means that
251 conventional pathway secreted SARS ORF8a is not glycosylated.

252

253 Next, we asked whether the glycosylation status of ORF8 is associated with the
254 release of pro-inflammatory factors. Calu-3 epithelial cells were infected with
255 SARS-CoV-2, and tunicamycin(35) or PNGase F was used to oppose the N-linked
256 glycosylation, respectively. Then purified ORF8 protein was added into the culture
257 medium of THP-1 DM cells for stimulation. The results showed that macrophages
258 stimulated with non-glycosylated ORF8 showed an elevated level of cytokine
259 secretion (Fig. 3F). Furthermore, we used plasmid transfection instead of
260 SARS-CoV-2 infection to validate this result. In line with previous results, a similar
261 upregulation in cytokine release was observed in the tunicamycin and PNGase F
262 treatment groups (Fig. 3G). In contrast, the pro-inflammatory factor expression of
263 Calu-3 cells transfected with SARS ORF8a-Flag plasmid did not change upon
264 tunicamycin or PNGase F treatment (Fig. S2D). Taken together, these results

265 suggested that glycosylation state of ORF8 is closely associated with the release of
266 pro-inflammatory factors.

267

268 **N-linked glycosylation at Asn78 impedes ORF8 binding to IL17RA**

269 In order to determine the specific glycosylation site of SARS-CoV-2 ORF8, we
270 collected the supernatant of SARS-CoV-2 infected Calu-3 epithelial cells and
271 performed high performance liquid chromatography-tandem mass spectrometry
272 (HPLC-MS/MS) for N-glycosylation site mapping (Fig. 4A). According to the
273 identification by MS, we found the Asparagine 78 (Asn78 or N78) of ORF8 protein to
274 be glycosylated (Fig. 4B). We further investigated the glycosylation site by creating a
275 SARS-CoV-2 variant carrying the ORF8 N78Q mutation. Following infection with a
276 SARS-CoV-2 ORF8-N78Q mutant, Calu-3 epithelial cells secreted a single form of
277 unglycosylated ORF8 (Fig. 4C). This finding was also validated by transfection of
278 exogenously expressed Flag-tagged N78Q ORF8 plasmid (Fig. 4C). Further, we
279 treated THP-1 DM cells with supernatant enriched from Calu-3 cells infected with
280 wild-type or the SARS-CoV-2 ORF8-N78Q mutant, respectively. In this context,
281 more pronounced cytokine release was observed in macrophages stimulated with the
282 ORF8-N78Q mutant protein (Fig. 4D). This result was further validated by exogenous
283 expression of wild-type ORF8 and N78Q mutants. Consistent with previous results,
284 transfection of N78Q mutant led to the excessive expression of pro-inflammatory
285 factors (Fig. 4E). These data show that unglycosylated ORF8, instead of glycosylated
286 ORF8, is involved in the inflammation response upon SARS-CoV-2 infection.

287

288 In our previous studies, we found that the interaction between ORF8 and host IL17RA
289 contributes to the formation of a cytokine storm(6). Here, we tested the effect of
290 ORF8 glycosylation on the activation of the IL-17 pathway. We found that ORF8
291 protein secreted from the SARS-CoV-2 ORF8-N78Q variant or Flag-tagged
292 ORF8-N78Q mutant, which could not be N-glycosylated at N78, exhibited stronger
293 binding to the IL17RA receptor compared to a wild-type control (Fig. 4F). Further,
294 the interaction between SARS-CoV-2 ORF8 and IL17RA was significantly increased
295 when PNGase F was used to remove glycosylation (Fig. 4G). However, ORF8-N78Q
296 showed consistently strong binding to IL17RA regardless of PNGase F treatment (Fig.
297 4G). We also tested the activation of NF- κ B signaling downstream of the IL-17
298 pathway(36). Consistently, the activation of NF- κ B signaling was positively
299 correlated with the binding affinity between ORF8 and IL17RA (Fig. S3A, B). Data
300 collected from plasmid transfection of Flag-tagged ORF8 mutant further validated this
301 result (Fig. 4H, S3C). To further confirm that the N-linked glycosylated ORF8 was
302 secreted via a conventional pathway, Brefeldin A or Monensin was used to pretreat
303 Calu-3 epithelial cells to block conventional secretory transport. As a result, inhibition
304 of Golgi-dependent vesicle transport decreased the interaction between ORF8 and
305 IL17RA in N78Q groups, because less ORF8 was secreted when ER-Golgi trafficking
306 was blocked (Fig. S3D, E); however, this inhibition did not affect the interaction
307 between ORF8 and IL17RA in control groups, mainly due to conventionally secreted
308 ORF8 was glycosylated (Fig. 4I, J, S3F, G).

309

310 Further, we prepared N-glycosylated ORF8 protein (ORF8-N-Glyc) *in vitro* and
311 stimulated THP-1 DM cells directly. The results showed that glycosylated ORF8
312 could not bind the IL17RA receptor (Fig. 5A), and that secretion of pro-inflammatory
313 factors was significantly reduced (Fig. 5B). These data indicated that
314 glycosylation-deficient ORF8 is capable of binding to IL17RA and subsequent
315 activation of the IL-17 pathway, thus promoting the cytokine storm. In order to further
316 verify the contribution of ORF8 glycosylation to cytokine release during
317 SARS-CoV-2 infection *in vivo*, we treated humanized ACE2 (hACE2) mice with
318 aerosols of synthetic ORF8 or ORF8-N-Glyc. Compared with control group, the
319 survival time of mice exposed to ORF8-N-Glyc was significantly prolonged (Fig. 5C).
320 We also observed very little inflammation in the lungs from mice treated with
321 ORF8-N-Glyc, while the lung lesions in unglycosylated ORF8-exposed mice were
322 much more severe (Fig. 5D). Additionally, mice treated with ORF8-N-Glyc secreted
323 decreased levels of cytokines and chemokines in lungs and livers (Fig. 5E, F). Taken
324 together, these data indicated that the N78 glycosylation of ORF8 participates in the
325 regulation of inflammatory response during SARS-CoV-2 infection.

326

327 **YIF1B is essential for the unconventional secretion of ORF8**

328 A substantial number of secreted eukaryotic proteins lacking classical signal peptides
329 (called leaderless cargoes) are released through unconventional secretion(37, 38). It
330 has been reported that channel proteins located on the ER-Golgi intermediate

331 compartment (ERGIC) might mediate translocation of leaderless cargoes into
332 transport vesicles(39). However, the driving factors of initial vesicle formation have
333 not yet been fully elucidated. Recent evidence suggests that autophagy contributes to
334 the formation of unconventional secretory vesicles(39-41). Therefore, we next
335 examined whether the unconventional secretion of ORF8 is regulated by autophagy.
336 Calu-3 epithelial cells were pretreated with Brefeldin A to block the conventional
337 secretory pathway, and then infected with SARS-CoV-2. Under the stimulation of
338 starvation or Rapamycin (an autophagy activator), the secretion of ORF8 increased
339 significantly (Fig. S4A). Autophagy inhibitor 3- Methyladenine (3-MA) or
340 Wortmannin (Wtm) could counteract the starvation-induced ORF8 secretion (Fig.
341 S4B). Consistently, knockdown of autophagy-related genes, such as *Atg5*, *Atg2a* or
342 *Atg2b*, also inhibited the release of ORF8 (Fig. S4C). Additionally, we observed
343 co-localization of ORF8 and ERGIC-53, indicating the possibility of ORF8
344 translocation into ERGIC (Fig. S4D). The proteinase K protection test also provided
345 evidence of vesicle-mediated ORF8 transportation (Fig. S4E). These data suggested
346 that SARS-CoV-2 ORF8 likely features an unconventional secretion pattern similar to
347 eukaryotic leaderless cargoes.

348
349 To further determine the channel protein that guides the translocation of ORF8 into an
350 unconventional secretion pattern, we performed mass spectrometry analysis to
351 identify proteins that interact with unglycosylated ORF8. To enrich as many potential
352 channel proteins on ORF8 transport vesicles as possible, dihydrofolate reductase

353 (DHFR)-tagged ORF8 was transfected into HEK-293FT cells pretreated with
354 aminopterin and Brefeldin A/Monensin as previously described (12)(Fig. S4F). Of the
355 156 potential interacting proteins, seven channel proteins appeared to be related to
356 cargo transport (Fig. S4G). We then screened the seven candidates using knockdown
357 strategy by siRNAs, and found that YIF1B was associated with the unconventional
358 secretion of ORF8 (Fig. S4G).

359

360 Next, we verified the interaction between ORF8 and YIF1B by immunoprecipitation.
361 Flag-tagged ORF8 was transfected into HEK-293FT cells and an interaction between
362 ORF8 and YIF1B was observed (Fig. 6A). The co-localization of exogenously
363 expressed HA-tagged YIF1B and Flag-tagged ORF8 was detected in HEK-293FT
364 cells by immunoprecipitation (Fig. 6B) and the Duolink proximity ligation assay (Fig.
365 6C). Further, endogenous YIF1B and virus-derived ORF8 were able to form a
366 complex in SARS-CoV-2 infected Calu-3 epithelial cells (Fig. 6D).

367

368 Then we generated YIF1B-deficient cells (YIF1B-KO) based on the Calu-3 cell line,
369 and found that unconventional secretion of ORF8 disappeared in absence of YIF1B;
370 however, exogenous supplementation of YIF1B by plasmid transfection rescued the
371 secretion of ORF8 (Fig. 6E, F). Moreover, cytokine release assays further proved that
372 YIF1B overexpression reconstituted the function of ORF8 protein in YIF1B-KO cells
373 (Fig. 6G). Likewise, ORF8 secretion and cytokine release data collected from
374 ORF8-Flag plasmid transfection further confirmed above findings (Fig. 6H-J). These

375 results indicated that the unconventional secretion pattern of SARS-CoV-2 ORF8
376 requires host YIF1B.

377

378 **The α 4 helix of YIF1B recognizes the β 8 sheet of ORF8 for interaction**

379 The structural domain of ORF8 protein, which is eight β -pleated sheets consisted by

380 165 amino acid chain, has been reported(42) (Fig. 7A). We constructed ORF8

381 $\Delta\beta$ 1- $\Delta\beta$ 8 deletion mutants, respectively. The results of co-immunoprecipitation

382 showed that an ORF8 mutant lacking the β 8 sheet could not bind to YIF1B (Fig. 7B).

383 Similarly, we observed that β 8 sheet-deleted ORF8 could not be secreted when the

384 conventional secretion pathway was blocked by Brefeldin A pretreatment (Fig. 7C, D).

385 Likewise, the cytokine release by THP-1 DM cells stimulated with supernatant proved

386 that β 8 sheet domain was closely associated with the unconventional secretory

387 pathway of ORF8 protein (Fig. 7E).

388

389 In order to understand how YIF1B mediates the recognition and secretion of leadless

390 cargoes, we constructed deletion mutants of five α helices located on the

391 transmembrane domains of YIF1B according to the structural predication

392 (<https://alphafold.ebi.ac.uk/entry/Q5BJH7>) (Fig. 7F). Co-immunoprecipitation results

393 showed that a α 4 helix deletion impaired the interaction between YIF1B and ORF8

394 (Fig. 7G). Next, we transfected exogenous YIF1B mutants into wild-type epithelial

395 Calu-3 cells. We found that the unconventional secretion of ORF8 increased

396 significantly in YIF1B mutants groups; this however was not observed in the $\Delta\alpha$ 4

397 mutant group (Fig. 7H-J). Further, after transfection of YIF1B mutants into
398 YIF1B-KO cells, the unconventional secretion of ORF8 was rescued by all YIF1B
399 mutants, except the $\Delta\alpha 4$ mutant (Fig. 7K-M). These data implied that the
400 unconventional secretion of ORF8 relies on the $\alpha 4$ helix of YIF1B and depends on its
401 presence in a dose-dependent manner (Fig. 7H-J).

402

403 Next, we asked whether YIF1B-guided unconventional secretion of leaderless ORF8
404 is driven by direct recognition of the $\beta 8$ sheet. To answer this question, we
405 constructed a 3CL pro mutant with a $\beta 8$ sheet fused to the C-terminus. Interestingly,
406 an interaction between 3CL pro- $\beta 8$ fusion and YIF1B was observed (Fig. 7N), and
407 secreted 3CL pro could be collected from culture supernatant (Fig. 7O). Collectively,
408 these evidences indicated that unconventional secretion of ORF8 is mediated by host
409 YIF1B through recognition and interaction between the $\beta 8$ sheet and $\alpha 4$ helix domain.

410

411 **YIF1B directly promotes the translocation of ORF8**

412 Since the interaction between ORF8 and YIF1B is important for the unconventional
413 secretion pattern of ORF8, we first looked for intracellular co-localization of ORF8
414 and YIF1B during SARS-CoV-2 infection. Immunofluorescence results showed that
415 full-length ORF8 and YIF1B did co-localized (Fig. 8A). However, neither an ORF8
416 $\beta 8$ sheet-deleted mutant nor a YIF1B $\alpha 4$ helix-deficient mutant co-localized with their
417 respective partner (Fig. 8B, C). Next, a proteinase K protection test was performed to
418 examine whether ORF8 transportation into vesicles relies on ORF8-YIF1B interaction.

419 Full-length ORF8-Flag or YIF1B truncations were transfected into YIF1B-KO cells as
420 indicated, the membrane pellets were collected by centrifugation and treated with
421 proteinase K or Triton X-100. The results showed that in YIF1B-deficient cells, ORF8
422 was not transported into vesicles, leading to its degradation by proteinase K (Fig. 8D).
423 On the contrary, ORF8 was able to resist the degradation by proteinase K when
424 YIF1B truncation was counteracted by transfection of YIF1B plasmids, except in case
425 of the $\Delta\alpha 4$ mutant (Fig. 8D).

426

427 Furthermore, we constructed an *in vitro* ORF8 transport system as previously
428 described(12). In this system, synthesized ORF8 was mixed with assembled
429 proteoliposomes, and HEK-293FT cell lysate without endomembrane was used as the
430 reaction buffer to promote the transport of ORF8 (Fig. 8E). A proteinase K protection
431 test showed that YIF1B mediated the transport of ORF8 into proteoliposomes in a
432 dose-dependent manner (Fig. 8F).

433

434 We also established a GFP fluorescence complementation system(43) to validate if
435 ORF8 resides in the same vesicle that also harbors YIF1B. ORF8 fused with GFP(11)
436 and YIF1B containing GFP(1-10) were co-transfected into HEK-293FT cells and flow
437 cytometry was used to measure the fluorescence emitted by the combination of ORF8
438 and YIF1B (Fig. 8G). When the amount of transfected ORF8 or YIF1B increased, an
439 elevation in fluorescence intensity was observed, suggesting that the binding rate of
440 ORF8-YIF1B complex increased in a concentration depended manner(Fig. 8H, I).

441 Collectively, these data clarified that YIF1B directly promotes the translocation of

442 ORF8 into vesicles for unconventional secretion.

443

444 **YIF1B regulates cytokine storm upon SARS-CoV-2 infection**

445 YIF1B regulates the translocation of SARS-CoV-2 ORF8 into vesicles, and thereby

446 promotes the unconventional secretion of unglycosylated ORF8 protein, which is

447 required for the downstream IL-17 signaling activation and release of

448 pro-inflammatory. To ascertain the biologic significance of our findings, we generated

449 YIF1B-deficient (*Yif1b*^{-/-}) mice in a hACE2 background (Fig. S5A-C). After

450 SARS-CoV-2 infection, the interaction between ORF8 and YIF1B disappeared (Fig.

451 9A), and ORF8 secretion was significantly decreased in alveolar epithelial cells

452 collected from these mice (Fig. 9B). In line with our expectations, supplementation of

453 exogenous YIF1B restored the secretion of ORF8 (Fig. 9B). Further, epithelial cells

454 obtained from *Yif1b*^{-/-} mice only secreted N-glycosylated ORF8, indicating a

455 deficiency of the unconventional secretory pathway (Fig. 9C). Consistently, ORF8

456 secreted from *Yif1b*^{-/-} epithelial cells neither bound the IL17RA receptor nor did it

457 trigger the downstream NF-κB pathway (Fig. 9D, E). These data again illustrated that

458 the unconventional secretory pathway mediated by YIF1B allows ORF8 to escape

459 host cell glycosylation, thus enabling activation of the IL-17 signaling pathway.

460

461 To further characterize the functional role of host YIF1B in the development of a

462 cytokine storm during SARS-CoV-2 infection, *Yif1b*^{-/-} hACE2 mice were intranasally

463 infected with 4×10^5 PFU plaque-forming units (PFU) of SARS-CoV-2. Compared to
464 the *Yif1b*^{+/+} littermates, the survival time of *Yif1b*^{-/-} mice infected with SARS-CoV-2
465 was significantly prolonged (Fig. 9F). The lungs of *Yif1b*^{-/-} mice showed only mild
466 inflammation compared to the extensive lung lesions observed in *Yif1b*^{+/+} mice (Fig.
467 9G). Further, we examined the viral loads and cytokine release in the spleens and
468 livers of *Yif1b*^{-/-} mice and their *Yif1b*^{+/+} littermates. In this assay, although the viral
469 loads showed no significant difference in the two groups (Fig. 9H), the cytokine
470 release in spleens and livers of *Yif1b*^{-/-} mice was strongly alleviated compared to the
471 control group (Fig. 9I, J). These results emphasize both the functional role of YIF1B
472 in the unconventional secretion of ORF8 and the mechanistic role of unconventional
473 ORF8 protein secretion in the development of a cytokine storm during SARS-CoV-2
474 infection.

475
476 Overall, we found that after invading host epithelial cells, SARS-CoV-2 ORF8 can be
477 secreted through both conventional and conventional secretory pathways. In the
478 conventional secretory pathway, ORF8 is N-glycosylated during the ER-Golgi
479 trafficking, consequently, extracellular ORF8 lost the ability to recognize the IL17RA
480 receptor of macrophages, likely due to steric hindrances imposed by N-glycosylation
481 at the Asn78 site. By contrast, ORF8 is recognized and then translocated into vesicles
482 directly by host YIF1B in an unconventional secretory pathway. Without experiencing
483 the conventional ER-Golgi trafficking, ORF8 protein does not become glycosylated.
484 Hence, extracellular ORF8 can be distributed through body fluid circulation and to get

485 in contact with macrophages, where unglycosylated ORF8 binds the IL17RA receptor
486 and activates the IL17 pathway and downstream NF- κ B signaling facilitating the
487 onset of a cytokine storm (Fig. 10).

488

489

490 **Discussion**

491 Understanding the specific functions of SARS-CoV-2 proteins is pivotal for us to
492 perceive the mechanisms which contribute to its high infectivity, fitness, and
493 virulence. Numerous studies unravelling the differential functions of structural
494 proteins have appeared recently(28, 44). However, it is worth noting that
495 non-structural and accessory proteins encoded by SARS-CoV-2 likewise play
496 significant roles in the regulation of the viral life cycle and also affect the immune
497 response of the host. For example, ORF3a has been reported to induce apoptosis and
498 promote lysosomal exocytosis-mediated viral egress(45, 46), while ORF6 protein of
499 SARS-CoV-2 hampers the induction of host interferon signaling(47).

500

501 ORF8, a non-conserved accessory protein, is likely to be associated with the unique
502 characteristics of SARS-CoV-2. According to clinical reports, ORF8 is highly
503 immunogenic, anti-ORF8 antibodies are formed in the early stage of infection(48) and
504 a significant T-cell response to ORF8 is observed in recovered patients(49). It is
505 further reported that an ORF8-deficient SARS-CoV-2 strain (Δ 382) in Singapore
506 displays a significant reduction in virulence(5). In a recent study, Zhang et al. reported

507 that SARS-CoV-2 ORF8 interacts with MHC-I, a marker protein located on the cell
508 surface, and activates the lysosomal degradation pathway, thus achieving escape from
509 immune surveillance by decreasing the expression of MHC I(50). These data indicate
510 the specific role of ORF8 in infectivity and pathogenicity of SARS-CoV-2.

511

512 Our previous work showed that SARS-CoV-2 ORF8 could interact with the IL17RA
513 receptor, thereby leading to IL-17 pathway activation and an increased secretion of
514 pro-inflammatory factors(6). Considering that IL17RA is a transmembrane protein
515 and ORF8 binds to the extracellular domain of IL17RA, as well as combining with
516 the existing evidences, we proposed that ORF8 might be a secretory protein that is
517 secreted into extracellular compartments. In this study, we show that SARS-CoV-2
518 ORF8 protein can be secreted by infected epithelial cells, which is supporting the role
519 of ORF8 as a cellular messenger between alveolar epithelial cells and macrophages in
520 the occurrence and development of a cytokine storm. Interestingly, we discovered that
521 ORF8 can be secreted through both a conventional and an unconventional secretory
522 pathway, and that ORF8 secreted via different pathways has different mechanistic
523 functions in SARS-CoV-2 infection. Specifically, conventionally secreted ORF8 is
524 N-glycosylated and loses the ability of binding the IL17RA receptor.
525 Unconventionally secreted ORF8 is undergoing the conventional ER-Golgi trafficking
526 pathway and consequently does not become glycosylated. Therefore, it is able to bind
527 the IL17RA receptor and activate IL-17 signaling induce the expression of
528 pro-inflammatory factors. The existence of this unique indirect cellular

529 communication mechanism, instead of virion release, during the course of
530 SARS-CoV-2 infection can at least partly explain why viral loads in patients are not
531 directly proportional to the severity of disease symptoms in COVID-19(51, 52).

532

533 In this study, we found that SARS ORF8a is also a secretory protein. Unlike
534 SARS-CoV-2 ORF8, SARS ORF8a could only be secreted through the conventional
535 secretory pathway. Notably, the conventionally secreted SARS ORF8a is not
536 glycosylated and is able to induce the release of pro-inflammatory factors. These
537 differences might be due to the fact that ORF8 is the only SARS-CoV-2 protein with
538 as low as approximate 20% homology to SARS(42). In this context, the very different
539 secretory pattern and functional role of ORF8 in SARS-CoV-2 can partly explain why
540 the disease spectrum of COVID-19 is different from that of SARS. Based on our data,
541 we propose a potential competition between host and guest regarding the ORF8
542 protein: Primitive SARS invades host cells and secretes ORF8 through the
543 conventional ER-Golgi trafficking pathway. ORF8 is not glycosylated in the Golgi
544 apparatus and can induce the release of pro-inflammatory factors. However, the host
545 does not just surrender to viral infection. During the evolutionary process, the host
546 blocks the induction of IL-17 signaling through ORF8 glycosylation to maintain
547 homeostasis. However, life finds a way; an evolved coronavirus develops a new
548 pathway to bypass the glycosylation modification and secrete unglycosylated ORF8
549 protein, thus regaining an advantageous position in this competition for the moment.
550 Nevertheless, this storyline needs to be validated by further studies.

551

552 In the current work, we identified YIF1B, a five-transmembrane protein, as a key
553 molecule that mediates transport of cargo into vesicles to facilitate the unconventional
554 secretion pattern of ORF8. Knockout of YIF1B in epithelial cells prevents the
555 unconventional secretion of ORF8, and exogenous supplementation of YIF1B rescues
556 the secretion of ORF8 even when Golgi apparatus is destructed by Brefeldin A. The *in*
557 *vitro* translocation assay proved that YIF1B promotes the translocation of ORF8 into
558 vesicles directly. Generally, the translocation process of leaderless cargoes into
559 vesicles depends on chaperones(53). For example, leaderless cargoes bind to
560 chaperone HSP90A that likely recognizes and unfolds the cargoes in the
561 TMED10-channeled unconventional protein secretion pathway(40). Whether the
562 translocation of leaderless ORF8 into vesicles needs chaperones in addition to the
563 YIF1B channel is not yet known. Notably, the proteinase K protection assays shows
564 that ORF8 cannot be translocated into vesicles without the supplementation of cell
565 lysates containing non-inner membranes. This result does suggest the necessity of
566 chaperones in the translocation of leaderless ORF8. It would be interesting to further
567 investigate the specific role of chaperones in the unconventional secretion of
568 SARS-CoV-2 ORF8.

569

570

571

572 **Materials and Methods**

573 **Ethic statements**

574 This study was carried out in strict accordance with the Guidelines for the Care and
575 Use of Animals of Chongqing University. All animal experimental procedures were
576 approved by the Animal Ethics Committees of the School of Life Sciences,
577 Chongqing University.

578

579 **Mice**

580 B6.Cg-Tg(K18-ACE2)2Prlmn/J mice (hACE2) were obtained from The Jackson
581 Laboratory. To generate YIF1B-deficient (*Yif1b*^{-/-}) mice based on K18-ACE2
582 transgenic background, we designed sgRNAs targeting the Exon 3-5 of *Yif1b*. Cas9
583 and sgRNAs (sgRNA1: CAGCTAACACGGTGGGTTGT, sgRNA2:
584 GAGGCCAAGAGCCATCAGAG) were co-injected into fertilized eggs of hACE2
585 mice. PCR followed by sequencing analysis and western blotting were used for
586 validation. All animal study protocols were reviewed and approved by Chongqing
587 University School of Life Sciences review boards for animal studies.

588

589 **Cell lines and coronavirus**

590 Calu-3 epithelial cells (HTB-55), Jurkat cells (Clone E6-1, TIB-152), THP-1 cells
591 (TIB-202), Vero E6 cells (CRL-1586) and Sf9 cells (CRL-1711) were purchased from
592 ATCC. HEK-293FT cells (R70007) were purchased from Thermo Fisher Scientific.
593 Differentiation of THP-1 monocytes to macrophages was induced by 15 ng/mL
594 phorbol 12-myristate 13-acetate (PMA) as previously described(54). *Ace2*^{-/-} Calu-3

595 epithelial cell line, *Il17ra*^{-/-} THP-1-derived macrophage cell line and YIF1B-KO
596 Calu-3 epithelial cell line were generated using CRISPR-Cas9 system with short
597 guide RNA sequences (*Ace2*^{-/-} cell line: ACAGTTAGACTACAATGAG; *Il17ra*^{-/-}
598 cell line: TGTCCATTGATGTGAGCCA; YIF1B-KO cell line:
599 GAGAGGCTGCAGGATAACTC). Murine alveolar epithelial cells (AECs) were
600 isolated using the method developed by Corti and colleagues with modifications(55,
601 56). Plasmid and siRNA transfections were performed using a LONZA
602 4D-Nucleofector system according to the manufacturer's instruction. The
603 SARS-CoV-2 virus was generated by using a reverse genetic method as previously
604 described(25-27). In brief, seven different DNA fragments spanning the entire
605 genome of SARS-CoV-2 (USA_WA1/2020 SARS-CoV-2 sequence, GenBank
606 accession No. MT020880) were synthesized by Beijing Genomics Institute (BGI,
607 Shanghai, China) and cloned into the pUC57 or pCC1 (kindly provided by Dr.
608 Yonghui Zheng) plasmid by standard molecular cloning methods. The sequences of
609 the F1~F7 fragments and the restriction enzymes used for digestion and ligation were
610 shown in our previous study(25). Full-length cDNA assembly and recombinant
611 SARS-CoV-2 virus recovery were performed as previously described(25-27). Virus
612 titer was determined using a standard TCID₅₀ assay. For the generation of
613 SARS-CoV-2 ORF8-N78Q variant, AAT→CAA nucleotide substitutions were
614 introduced into a subclone of pUC57-F7 containing the ORF8 gene of the
615 SARS-CoV-2 wild-type infectious clone by overlap-extension PCR. Primers are as
616 follows: F- TCAGTACATCGATATCGGTCAATAT, R-

617 GTAAACAGGAAACTGTATATTGACC.

618

619 **Viral infection**

620 Specific-pathogen-free, ten-week-old male mice were inoculated intranasally with
621 SARS-CoV-2 virus with 4×10^5 plaque-forming units (PFU). Cells were infected with
622 SARS-CoV-2 virus at a dosage of 10^5 TCID₅₀/mL within the indicated time. Cell
623 culture supernatant obtained from infected epithelial cells was filtered by Ultipor VF
624 Grade UDV20 Virus Removal Filter Cartridges (PALL) to remove virion, and used
625 for macrophage stimulation. All experiments with infectious virus were performed
626 under biosafety level 3 (BSL3+) conditions.

627

628 **Collection of secretory proteins and immunoblot**

629 Cell culture medium was collected and centrifuged twice to remove cell debris. The
630 supernatant was concentrated through a 10 kDa Amicon-Ultra centrifugal tube
631 (Millipore) and prepared for immunoblot. GAPDH was used to indicate the absence
632 of cell lysates. Immunoblot analysis was performed as previously described(57). Blots
633 were probed with the indicated antibodies: anti-ORF8 (NBP3-05720), anti-GAPDH
634 (NBP2-27103) (Novus Biologicals), anti-3CL pro (GTX135470) (GeneTex),
635 anti-NEF (MA1-71507), anti-IL17RA (PA5-47199) (Thermo Fisher Scientific),
636 anti-GFP (ab6556), anti-YIF1B (ab188127), anti-SEC22B (ab241585), anti-V5
637 (ab9137) (Abcam), anti-PDI (2446) (Cell Signaling Technology), anti-Flag (AF0036),
638 anti-His (AF5060), anti-GST (AF5063), anti-HA (AF0039) (Beyotime

639 Biotechnology).

640

641 **Enzyme linked immunosorbent assay**

642 Cell culture supernatant was purified by centrifugation, and assayed by enzyme linked
643 immunosorbent assays (ELISA). ORF8 antibody (NBP3-05720, Novus Biologicals)
644 was coated with blank ELISA plates in carbonate buffer to prepare ELISA kit.

645 Cytokine and chemokine ELISA kits were purchased from eBiosciences (Thermo
646 Fisher Scientific).

647

648 **Block of conventional secretory pathway**

649 Brefeldin A (00-4506-51, eBioscience, 3 µg/mL) or Monensin (00-4505-51,
650 eBioscience, 2 µM) was added in the culture medium of epithelial cells for 2 hours to
651 inhibit the ER-Golgi trafficking and block the ER-Golgi conventional secretion
652 pathway.

653

654 **N-linked glycosylation identification by HPLC-MS/MS**

655 N-linked glycosylation identification of SARS-CoV-2 ORF8 protein was performed
656 as previously described with slight modifications(58). Firstly, Calu-3 epithelial cells
657 were infected by SARS-CoV-2 with/without Brefeldin A or Monensin pretreatment.

658 The supernatant was collected and concentrated through a 10 kDa Amicon-Ultra
659 centrifugal tube (Millipore). Then, the N-glycopeptides were enriched with
660 Zic-HILIC (Fresh Bioscience), eluted and dried for deglycosylation. Enriched

661 N-glycopeptides were digested using PNGase F dissolved in 50 mM NH₄HCO₃ for 2
662 hours at 37 °C to remove N-linked glycosylation. Finally, deglycosylated peptides
663 were dissolved in 0.1% FA for tandem mass spectrum analysis. MS1 was analyzed at
664 an Orbitrap resolution of 120,000 using a scan range (m/z) of 800 to 2000
665 (N-glycopeptides before and after enrichment), or 350 to 1550 (deglycosylated
666 peptides). The RF lens, AGC target, maximum injection time, and exclusion duration
667 were 30%, 2.0 e⁴, 100 ms and 15 s, respectively. MS2 was analyzed with an isolation
668 window (m/z) of 2 at an Orbitrap resolution of 15,000. The AGC target, maximum
669 injection time, and the HCD type were standard, 250 ms, and 30%, respectively.

670

671 **Deglycosylation assays**

672 Tunicamycin (12819, Cell Signaling Technology, 2μg/mL) was added into epithelial
673 cells to prevent N-linked glycosylation. PNGase F (P0704, NEB, 1,000 units/μg
674 protein) was used to remove the N-linked glycosylation in purified ORF8 protein. 1
675 μg glycoprotein, 2 μL GlycoBuffer 2 (10×), 2 μL PNGase F and H₂O were mixed to
676 form a 20 μL mixture. The mixture was incubated at 37°C for 8 hours, followed by
677 western blotting analysis. To remove O-linked glycosylation, purified proteins were
678 directly digested by O-glycosidase (P0733, NEB, 4,000 units/μg protein) and α2-3, 6,
679 8, 9 Neuraminidase A (P0722, NEB, 4 units/μg protein). 10 μg glycoprotein, 1 μL
680 10× Glycoprotein Denaturing Buffer and H₂O were combined to make a 10 μL
681 mixture. The glycoprotein was denatured by heating the mixture at 100°C for 10 min.
682 Then, 2 μL 10× GlycoBuffer 2, 2 μL 10% NP40, 2 μL α2-3, 6, 8, 9 Neuraminidase A,

683 1 μ L O-Glycosidase and H₂O were mixed to form a total volume of 20 μ L and
684 incubated at 37°C for 4 hours, followed by western blotting analysis.

685

686 **Peptide synthesis and artificial glycosylation modification**

687 SARS-CoV-2 ORF8 peptide was synthesized according to the NCBI published
688 sequence (accession number: YP_009724396.1). Fmoc-L-Asn
689 ((Ac)3- β -D-GlcNAc)-OH modification was performed by Shanghai Science Peptide
690 Biological Technology Co., Ltd. ORF8 peptides with or without N-glycosylation were
691 dissolved in 40 μ L DMSO and diluted with PBS buffer for cell stimulation (1 μ g/mL)
692 or mice aerosol infection (10 μ g/g).

693

694 **Identification of the interaction channel proteins of ORF8**

695 DHFR assay followed by HPLC-MS/MS was used to screen the channel proteins
696 mediating ORF8 translocation in an unconventional secretion pathway as previously
697 described(12). Calu-3 cells expressing ORF8-Flag-DHFR were treated with Brefeldin
698 A (3 μ g/mL) or Monensin (2 μ M) to inhibit conventional secretion pathways.
699 Aminopterin (15 μ M) was added to inhibit DHFR unfolding. After crosslinking,
700 membrane fractions were collected, lysed and immunoprecipitated with anti-Flag
701 beads for HPLC-MS/MS analysis.

702

703 **Duolink PLA assay**

704 Duolink PLA assay was performed according to the kit manual (Duolink In Situ

705 Detection Reagents Red, DUO92008, Sigma). In brief, Flag-tagged ORF8 and
706 HA-tagged YIF1B were co-transfected into HEK-293FT cells. After 12 hours, cells
707 were fixed with 4% paraformaldehyde (PFA) for 20 min and permeabilized with 0.2%
708 Triton X-100. Next, the fixed cells were blocked, incubated with antibodies and PLA
709 probes according to the protocol. Images were captured followed by quantification
710 using Image J software.

711

712 ***In vitro* translocation assay**

713 Purified YIF1B proteins (NCBI accession number: NP_001034761.1) was
714 synthesized by MembraneMaxTM cell-free protein synthesis system according to the
715 manufacturers' protocol (A10633, Thermo Fisher Scientific). Purified ORF8 protein
716 was expressed in baculovirus expression vector system (Thermo Fisher Scientific). In
717 brief, ORF8 protein-coding sequence without signal peptide was optimized according
718 to the insect cell codon preference, and synthesized by Sangon Biotech. The
719 Asparagine 78 was mutated to Glutamine to prevent glycosylation. Then, synthesized
720 ORF8 sequence was amplified by PCR and inserted into a pFastBac HT A plasmid
721 (Thermo Fisher Scientific). Recombinant pFastBac-ORF8 plasmid was transformed
722 into DH10Bac-competent cells to obtain Bacmid-ORF8, which was transfected into
723 Sf9 cells to produce ORF8 protein. Total lipids were extracted from HEK-293FT cells
724 as previously described(12). Purified YIF1B and lipids were reconstituted into
725 proteolioposomes. To be specific, lipids were repeatedly frozen and thawed in a 42°C
726 water bath for 10 times. Triton X-100 was used to dilute lipids to a final concentration

727 of 0.05%, and the lipid solution was rotated at 4°C for 30 min. Then, the purified
728 YIF1B protein was added into the lipid solution and rotated for 1 hour, followed by
729 incubation with Biobeads SM2 (Bio-Rad Laboratories) to absorb the detergent. After
730 centrifugation to remove the beads, a membrane flotation procedure was performed to
731 collect top fractions containing proteolioposomes. Next, proteolioposomes were
732 mixed with ORF8 protein in HEK-293FT lysates (whole cell lysates were centrifuged
733 at 1,000×g for 10 min and the supernatant was ultra-centrifuged at 100,000×g for 40
734 min to remove endomembrane) for 1 hour. The mixture was centrifuged, aliquoted
735 into three parts, and collected for proteinase K protection test.

736

737 **Proteinase K protection test**

738 Proteinase K protection test was performed as previously described(40). Briefly, cells
739 were harvested and lysed in HB1 buffer (20 mM HEPES-KOH, pH 7.2, 400 mM
740 sucrose, and 1 mM EDTA) with 0.3 mM DTT and protease inhibitors. After
741 centrifugation, supernatant was ultra-centrifuged at 100,000×g for 40 min to collect
742 the total membrane pellet, followed by membrane flotation assay. The membrane
743 fraction floating on the top was collected and divided into three parts (without
744 proteinase K, with proteinase K, or with proteinase K and 0.5% Triton X-100). The
745 reactions were performed on ice and stopped by adding PMSF and SDS loading
746 buffer. The samples were immediately heated at 98°C for 5 min, followed by
747 SDS-PAGE. Protein disulfide isomerase (PDI) and a vesicle trafficking protein,
748 SEC22 Homolog B (SEC22B), were used as the positive and negative control,

749 respectively.

750

751 **H&E staining**

752 Mice were anaesthetized with isoflurane, and lung lobes were harvested at indicated
753 time points. Tissues were fixed with 10% PFA for more than 24 hours and embedded
754 in paraffin. The paraffin blocks were cut into 2 μ m-thick sections and stained using a
755 standard Hematoxylin and eosin (H&E) procedure.

756

757 **Statistical Analysis**

758 Sample size was based on empirical data from pilot experiments. The investigators
759 were blinded during data collection and analysis. A value of $P < 0.05$ was considered
760 significant.

761

762 **Acknowledgments**

763 This work was supported by the National Natural Science Foundation of China,
764 SGC's Rapid Response Funding for COVID-19 (C-0002), National Natural Science
765 Foundation of China (No. 81970008, 82000020, 31702205), the Fundamental
766 Research Funds for the Central Universities (No. 2021CDJZYJH-002,
767 2019CDYGZD009 and 2020CDJYGRH-1005), Natural Science Foundation of
768 Chongqing, China (cstc2020jcyj-msxmX0460 and cstc2020jcyj-bshX0105) and
769 Chongqing Talents: Exceptional Young Talents Project (No.
770 cstc2021ycjh-bgzxm0099). The funders had no role in study design, data collection

771 and analysis, decision to publish, or preparation of the manuscript.

772

773 **Author contributions**

774 H. Wu, X. Lin and B. Fu conceived and designed the study. H. Wu, X. Lin, B. Fu, Y.
775 Xiong, N. Xing, W. Xue, D. Guo, M. Y. Zaky, K. C. Pavani, D. Kunec and J. Trimpert
776 performed the experiments. H. Wu, X. Lin and B. Fu analyzed the data. H. Wu, X. Lin,
777 B. Fu and J. Trimpert wrote the manuscript. All authors read and approved the final
778 manuscript.

779

780 **Conflict of Interest**

781 The authors declare that no conflict of interest exists.

782

783

784 **References**

- 785 1. L. Yang *et al.*, The signal pathways and treatment of cytokine storm in COVID-19. *Signal
786 Transduct Target Ther* **6**, 255 (2021).
- 787 2. C. Huang *et al.*, Clinical features of patients infected with 2019 novel coronavirus in Wuhan,
788 China. *Lancet* **395**, 497-506 (2020).
- 789 3. X. Tang *et al.*, On the origin and continuing evolution of SARS-CoV-2. *Natl Sci Rev* **7**,
790 1012-1023 (2020).
- 791 4. D. Muth *et al.*, Attenuation of replication by a 29 nucleotide deletion in SARS-coronavirus
792 acquired during the early stages of human-to-human transmission. *Sci Rep* **8**, 15177 (2018).
- 793 5. B. E. Young *et al.*, Effects of a major deletion in the SARS-CoV-2 genome on the severity of
794 infection and the inflammatory response: an observational cohort study. *Lancet* **396**, 603-611
795 (2020).
- 796 6. X. Lin *et al.*, ORF8 contributes to cytokine storm during SARS-CoV-2 infection by activating
797 IL-17 pathway. *iScience* **24**, 102293 (2021).
- 798 7. P. Bhadra, V. Helms, Molecular Modeling of Signal Peptide Recognition by Eukaryotic Sec
799 Complexes. *Int J Mol Sci* **22**, (2021).
- 800 8. J. McCaughey, D. J. Stephens, ER-to-Golgi Transport: A Sizeable Problem. *Trends in cell biology*

801 29, 940-953 (2019).

802 9. R. Z. Murray, J. L. Stow, Cytokine Secretion in Macrophages: SNAREs, Rabs, and Membrane
803 Trafficking. *Front Immunol* **5**, 538 (2014).

804 10. V. Malhotra, Unconventional protein secretion: an evolving mechanism. *The EMBO journal* **32**,
805 1660-1664 (2013).

806 11. J. P. Steringer, W. Nickel, A direct gateway into the extracellular space: Unconventional
807 secretion of FGF2 through self-sustained plasma membrane pores. *Seminars in cell &*
808 *developmental biology* **83**, 3-7 (2018).

809 12. M. Zhang *et al.*, A Translocation Pathway for Vesicle-Mediated Unconventional Protein
810 Secretion. *Cell* **181**, 637-652 e615 (2020).

811 13. R. P. McNamara *et al.*, Nef Secretion into Extracellular Vesicles or Exosomes Is Conserved
812 across Human and Simian Immunodeficiency Viruses. *mBio* **9**, (2018).

813 14. N. Mukhamedova *et al.*, Exosomes containing HIV protein Nef reorganize lipid rafts
814 potentiating inflammatory response in bystander cells. *PLoS Pathog* **15**, e1007907 (2019).

815 15. M. Z. Mehboob, M. Lang, Structure, function, and pathology of protein
816 O-glycosyltransferases. *Cell Death Dis* **12**, 71 (2021).

817 16. K. W. Moremen, M. Tiemeyer, A. V. Nairn, Vertebrate protein glycosylation: diversity,
818 synthesis and function. *Nat Rev Mol Cell Biol* **13**, 448-462 (2012).

819 17. K. T. Schjoldager, Y. Narimatsu, H. J. Joshi, H. Clausen, Global view of human protein
820 glycosylation pathways and functions. *Nat Rev Mol Cell Biol* **21**, 729-749 (2020).

821 18. W. Chen, Y. Zhong, Y. Qin, S. Sun, Z. Li, The evolutionary pattern of glycosylation sites in
822 influenza virus (H5N1) hemagglutinin and neuraminidase. *PLoS One* **7**, e49224 (2012).

823 19. S. S. L. Yap, T. Nguyen-Khuong, P. M. Rudd, S. Alonso, Dengue Virus Glycosylation: What Do
824 We Know? *Front Microbiol* **8**, 1415 (2017).

825 20. A. J. Behrens, M. Crispin, Structural principles controlling HIV envelope glycosylation. *Curr
826 Opin Struct Biol* **44**, 125-133 (2017).

827 21. D. L. Carbaugh, H. M. Lazear, Flavivirus Envelope Protein Glycosylation: Impacts on Viral
828 Infection and Pathogenesis. *Journal of virology* **94**, (2020).

829 22. W. Tian *et al.*, O-glycosylation pattern of the SARS-CoV-2 spike protein reveals an
830 "O-Follow-N" rule. *Cell research* **31**, 1123-1125 (2021).

831 23. Q. Li *et al.*, The Impact of Mutations in SARS-CoV-2 Spike on Viral Infectivity and Antigenicity.
832 *Cell* **182**, 1284-1294 e1289 (2020).

833 24. Y. Watanabe, J. D. Allen, D. Wrapp, J. S. McLellan, M. Crispin, Site-specific glycan analysis of
834 the SARS-CoV-2 spike. *Science* **369**, 330-333 (2020).

835 25. H. Wu *et al.*, Nucleocapsid mutations R203K/G204R increase the infectivity, fitness, and
836 virulence of SARS-CoV-2. *Cell Host Microbe*, (2021).

837 26. J. A. Plante *et al.*, Spike mutation D614G alters SARS-CoV-2 fitness. *Nature* **592**, 116-121
838 (2021).

839 27. X. Xie *et al.*, An Infectious cDNA Clone of SARS-CoV-2. *Cell Host Microbe* **27**, 841-848 e843
840 (2020).

841 28. Z. Ke *et al.*, Structures and distributions of SARS-CoV-2 spike proteins on intact virions. *Nature*
842 **588**, 498-502 (2020).

843 29. Q. Wang *et al.*, Structural and Functional Basis of SARS-CoV-2 Entry by Using Human ACE2.
844 *Cell* **181**, 894-904 e899 (2020).

845 30. S. Lin, S. Pandruvada, H. Yu, Inhibition of Sphingosine-1-Phosphate Receptor 2 by JTE013
846 Promoted Osteogenesis by Increasing Vesicle Trafficking, Wnt/Ca(2+), and BMP/Smad
847 Signaling. *Int J Mol Sci* **22**, (2021).

848 31. E. R. McGlone *et al.*, Receptor Activity-Modifying Protein 2 (RAMP2) alters glucagon receptor
849 trafficking in hepatocytes with functional effects on receptor signalling. *Mol Metab* **53**,
850 101296 (2021).

851 32. X. Zhang, Y. Wang, Nonredundant Roles of GRASP55 and GRASP65 in the Golgi Apparatus and
852 Beyond. *Trends in biochemical sciences* **45**, 1065-1079 (2020).

853 33. Y. Huang *et al.*, FUT8-mediated aberrant N-glycosylation of B7H3 suppresses the immune
854 response in triple-negative breast cancer. *Nature communications* **12**, 2672 (2021).

855 34. C. E. Martin *et al.*, Posttranslational modifications of serine protease TMPRSS13 regulate
856 zymogen activation, proteolytic activity, and cell surface localization. *The Journal of biological
857 chemistry* **297**, 101227 (2021).

858 35. X. Wang *et al.*, ER stress promotes HBV production by enhancing utilization of the
859 autophagosome- multivesicular body axis. *Hepatology*, (2021).

860 36. M. Akbar *et al.*, Translational targeting of inflammation and fibrosis in frozen shoulder:
861 Molecular dissection of the T cell/IL-17A axis. *Proc Natl Acad Sci U S A* **118**, (2021).

862 37. W. Nickel, C. Rabouille, Mechanisms of regulated unconventional protein secretion. *Nat Rev
863 Mol Cell Biol* **10**, 148-155 (2009).

864 38. C. Rabouille, Pathways of Unconventional Protein Secretion. *Trends in cell biology* **27**,
865 230-240 (2017).

866 39. L. Liu, M. Zhang, L. Ge, Protein translocation into the ERGIC: an upstream event of secretory
867 autophagy. *Autophagy* **16**, 1358-1360 (2020).

868 40. M. Zhang, S. J. Kenny, L. Ge, K. Xu, R. Schekman, Translocation of interleukin-1beta into a
869 vesicle intermediate in autophagy-mediated secretion. *Elife* **4**, (2015).

870 41. S. Subramani, V. Malhotra, Non-autophagic roles of autophagy-related proteins. *EMBO Rep*
871 **14**, 143-151 (2013).

872 42. T. G. Flower *et al.*, Structure of SARS-CoV-2 ORF8, a rapidly evolving immune evasion protein.
873 *Proc Natl Acad Sci U S A* **118**, (2021).

874 43. D. Kamiyama *et al.*, Versatile protein tagging in cells with split fluorescent protein. *Nature
875 communications* **7**, 11046 (2016).

876 44. L. Zhang *et al.*, Crystal structure of SARS-CoV-2 main protease provides a basis for design of
877 improved alpha-ketoamide inhibitors. *Science* **368**, 409-412 (2020).

878 45. D. Chen *et al.*, ORF3a of SARS-CoV-2 promotes lysosomal exocytosis-mediated viral egress.
879 *Dev Cell*, (2021).

880 46. Y. Ren *et al.*, The ORF3a protein of SARS-CoV-2 induces apoptosis in cells. *Cellular & molecular
881 immunology* **17**, 881-883 (2020).

882 47. I. Kimura *et al.*, Sarbecovirus ORF6 proteins hamper induction of interferon signaling. *Cell Rep*
883 **34**, 108916 (2021).

884 48. A. Hachim *et al.*, ORF8 and ORF3b antibodies are accurate serological markers of early and
885 late SARS-CoV-2 infection. *Nat Immunol* **21**, 1293-1301 (2020).

886 49. A. Grifoni *et al.*, Targets of T Cell Responses to SARS-CoV-2 Coronavirus in Humans with
887 COVID-19 Disease and Unexposed Individuals. *Cell* **181**, 1489-1501 e1415 (2020).

888 50. Y. Zhang *et al.*, The ORF8 protein of SARS-CoV-2 mediates immune evasion through

889 51. down-regulating MHC-Iota. *Proc Natl Acad Sci U S A* **118**, (2021).

890 51. K. K. To *et al.*, Temporal profiles of viral load in posterior oropharyngeal saliva samples and
891 serum antibody responses during infection by SARS-CoV-2: an observational cohort study.
892 *Lancet Infect Dis* **20**, 565-574 (2020).

893 52. F. X. Lescure *et al.*, Clinical and virological data of the first cases of COVID-19 in Europe: a case
894 series. *Lancet Infect Dis* **20**, 697-706 (2020).

895 53. S. Kaushik, A. M. Cuervo, Chaperone-mediated autophagy: a unique way to enter the
896 lysosome world. *Trends in cell biology* **22**, 407-417 (2012).

897 54. I. Pantazi *et al.*, SARS-CoV-2/ACE2 Interaction Suppresses IRAK-M Expression and Promotes
898 Pro-Inflammatory Cytokine Production in Macrophages. *Front Immunol* **12**, 683800 (2021).

899 55. M. Corti, A. R. Brody, J. H. Harrison, Isolation and primary culture of murine alveolar type II
900 cells. *Am J Respir Cell Mol Biol* **14**, 309-315 (1996).

901 56. L. Cakarova *et al.*, Macrophage tumor necrosis factor-alpha induces epithelial expression of
902 granulocyte-macrophage colony-stimulating factor: impact on alveolar epithelial repair. *Am J*
903 *Respir Crit Care Med* **180**, 521-532 (2009).

904 57. B. Fu *et al.*, MiR-342 controls Mycobacterium tuberculosis susceptibility by modulating
905 inflammation and cell death. *EMBO Rep* **22**, e52252 (2021).

906 58. Y. Zhang *et al.*, Site-specific N-glycosylation Characterization of Recombinant SARS-CoV-2
907 Spike Proteins. *Mol Cell Proteomics*, 100058 (2020).

908

909 **Figure legends**

910 **Figure 1 SARS-CoV-2 ORF8 can be secreted by epithelial cells**

911 (A) Schematic diagram of SARS-CoV-2 infectious cDNA clone generated by a
912 reverse genetic system. The cDNA fragments F1-F7 were synthesized and assembled
913 into full-length SARS-CoV-2 cDNA, and RNA transcription, electroporation, and
914 virus production were carried out in Vero E6 cells.

915 (B) Schematic diagram of SARS-CoV-2 infection model. Calu-3 epithelial cells were
916 infected with SARS-CoV-2 for 12 hours at a dosage of 10^5 TCID₅₀/mL. Cell culture
917 supernatant was centrifuged and divided into two parts for western blotting and
918 ELISA, respectively.

919 (C) The secretion of ORF8 in (B) was detected by western blotting and ELISA.

920 Representative images from n = 3 biological replicates are shown. Data in histogram

921 are shown as the mean \pm s.e.m. of n = 3 biological replicates.

922 (D) Jurkat cells and Calu-3 epithelial cells were infected with HIV-1 and
923 SARS-CoV-2 for 12 hours at a dosage of 10^5 TCID₅₀/mL. The secretion of ORF8, Nef
924 and 3CL pro was detected by western blotting. Representative images from n = 3
925 biological replicates are shown.

926 (E) Schematic diagram of time-dependent ORF8 secretion upon SARS-CoV-2
927 infection. After 12 hours of SARS-CoV-2 infection, cell culture medium was replaced,
928 and the amount of ORF8 protein in the supernatant was detected by ELISA every 2
929 hours. Data are shown as the mean \pm s.e.m. of n = 3 biological replicates.

930 (F-H) Schematic diagram of ORF8-deleted SARS-CoV-2 variant (F). ORF8 coding
931 sequence was deleted from the cDNA of F7 fragment. SARS-CoV-2 Δ ORF8 variant
932 was used to infect Calu-3 cells, THP-1 DM cells, and the co-culture system at a
933 dosage of 10^5 TCID₅₀/mL. The secretion of cytokines and chemokines related to
934 cytokine storm was detected by ELISA (G, H). Data are shown as the mean \pm s.e.m.
935 of n = 3 biological replicates (G, H).

936 (H) Calu-3 Ace2^{+/+}, Calu-3 Ace2^{-/-}, THP-1 DM *Il17ra*^{+/+} and THP-1 DM *Il17ra*^{-/-} cells
937 were used to form four kinds of culture systems. The secretion of cytokines and
938 chemokines in different cell culture systems was detected by ELISA. Data are shown
939 as the mean \pm s.e.m. of n = 3 biological replicates.

940 Unpaired two-tailed Student *t* test (C) and one-way ANOVA followed by Bonferroni
941 post *hoc* test (G, I) were used for data analysis. *, p < 0.05, **, p < 0.01.

942

943 **Figure 2 SARS-CoV-2 ORF8, rather than SARS ORF8, has an unconventional
944 secretion pattern**

945 (A) Structures of SARS-CoV-2 ORF8 and its signal peptide-deleted mutant.
946 (B, C) Full-length SARS-CoV-2 ORF8 or its signal peptide-deleted mutant were
947 transfected into Calu-3 cells or HEK-293FT cells. The secretion of ORF8 was
948 detected by western blotting (B) and ELISA (C). Representative images from n = 3
949 biological replicates are shown (B). Data are shown as the mean \pm s.e.m. of n = 3
950 biological replicates (C).

951 (D, E) Brefeldin A (3 μ g/mL) or Monensin (2 μ M) was used to pretreat Calu-3 cells
952 (D) or HEK-293FT cells (E) for 2 hours. Full-length SARS-CoV-2 ORF8 was
953 transfected into pretreated cells. After 12 hours, the secretion of ORF8 was detected
954 by western blotting. Representative images from n = 3 biological replicates are
955 shown.

956 (F) Structures of SARS ORF8a and its signal peptide-deleted mutant.
957 (G) Full-length SARS ORF8a or its signal peptide-deleted mutant were transfected
958 into Calu-3 cells or HEK-293FT cells. The secretion of ORF8a was detected by
959 western blotting. Representative images from n = 3 biological replicates are shown.
960 (H, I) Brefeldin A (3 μ g/mL) or Monensin (2 μ M) was used to pretreat Calu-3 cells (H)
961 or HEK-293FT cells (I) for 2 hours. Full-length SARS ORF8a was transfected into
962 pretreated cells. After 12 hours, the secretion of ORF8a was detected by western
963 blotting. Representative images from n = 3 biological replicates are shown.

964 (J) Structures of SARS-CoV-2 ORF8 mutant with signal peptide from SARS ORF8a

965 (with SARS-Signal), and SARS ORF8a mutant with signal peptide from
966 SARS-CoV-2 ORF8 (with SARS-CoV-2-Signal).
967 (K) Brefeldin A (3 μ g/mL) or Monensin (2 μ M) was used to pretreat Calu-3 cells for 2
968 hours. SARS-CoV-2 ORF8 with SARS-Signal and SARS ORF8a with
969 SARS-CoV-2-Signal were transfected into pretreated Calu-3 cells. After 12 hours, the
970 secretion of ORF8 was detected by western blotting. Representative images from $n =$
971 3 biological replicates are shown.
972 Unpaired two-tailed Student *t* test (C) was used for data analysis. *, $p < 0.05$, **, $p <$
973 0.01.

974

975 **Figure 3 Unconventional secretion of ORF8 induces cytokine storm**
976 (A) Schematic diagram of unconventional secretion model upon SARS-CoV-2
977 infection. Brefeldin A (3 μ g/mL) or Monensin (2 μ M) was used to pretreat Calu-3
978 cells for 2 hours, followed by SARS-CoV-2 infection for 12 hours at a dosage of 10^5
979 TCID₅₀/mL, or Flag-tagged ORF8 plasmid transfection for 12 hours. The supernatant
980 was collected to stimulate THP-1 DM cells.

981 (B) The secretion of ORF8 in (A) was detected by ELISA. Data are shown as the
982 mean \pm s.e.m. of $n = 3$ biological replicates.

983 (C, D) The release of cytokines and chemokines in (A) was detected by ELISA. Data
984 are shown as the mean \pm s.e.m. of $n = 3$ biological replicates.

985 (E) PNGase F (1,000 units/ μ g protein), O-Glycosidase (4,000 units/ μ g protein) or
986 α 2-3, 6, 8, 9 Neuraminidase A (4 units/ μ g glycoprotein) was added into the purified

987 SARS-CoV-2 ORF8 protein to release glycans. Western blotting was used to detect
988 the glycosylation of ORF8 protein. Representative images from n = 3 biological
989 replicates are shown.
990 (F, G) Calu-3 cells were infected with SARS-CoV-2 (F) or transfected with ORF-Flag
991 plasmids (G). Tunicamycin (2 μ g/mL) was added into Calu-3 cells for 2 hours to
992 prevent N-linked glycosylation; PNGase F (1,000 units/ μ g protein) was used to
993 remove the N-linked glycosylation in purified ORF8 protein. After deglycosylation
994 assays, the cell culture supernatant or purified ORF8 protein was used to stimulate
995 THP-1 DM cells. After 12 hours, the release of cytokines and chemokines was
996 detected by ELISA. Data are shown as the mean \pm s.e.m. of n = 3 biological
997 replicates.
998 One-way ANOVA followed by Bonferroni post *hoc* test (B-D, F, G) was used for data
999 analysis. *, p < 0.05, **, p < 0.01. Abbreviations: n.s., not significant.
1000

1001 Figure 4 **ORF8 N78 glycosylation blocks its interaction with IL17RA**
1002 (A) Schematic diagram of glycosylation identification based on HPLC-MS/MS.
1003 DMSO (control), Brefeldin A (3 μ g/mL) or Monensin (2 μ M) was used to pretreat
1004 Calu-3 cells for 2 hours. The supernatant was collected for HPLC-MS/MS analysis.
1005 (B) SARS-CoV-2 ORF8 secreted through conventional pattern has N78 glycosylation.
1006 An increase of 0.002989 Da of Asn residue was used to determine N-linked
1007 glycosylation.
1008 (C-E) Calu-3 cells were infected with SARS-CoV-2 variant carrying ORF8 N78Q

1009 mutant (C, D), or transfected with ORF8 N78Q plasmids (C, E). After 12 hours, the
1010 supernatant was collected and divided into two parts. One part was used to purify
1011 ORF8 protein, followed by PNGase F digestion and western blotting (C); the other
1012 part was used to stimulate THP-1 DM cells for 12 hours, followed by detection of
1013 cytokines and chemokines by ELISA (D, E). Representative images from n = 3
1014 biological replicates are shown (C). Data are shown as the mean ± s.e.m. of n = 3
1015 biological replicates (D, E).

1016 (F) Calu-3 cells were infected with SARS-CoV-2 ORF8-N78Q variant, or transfected
1017 with ORF8-N78Q plasmids. Twelve hours later, the supernatant was used to stimulate
1018 THP-1 DM cells for another 12 hours. The interaction of ORF8 and IL17RA was
1019 detected by co-immunoprecipitation. Representative images from n = 3 biological
1020 replicates are shown.

1021 (G, H) Calu-3 cells were infected with SARS-CoV-2 ORF8-N78Q variant (G), or
1022 transfected with ORF8-N78Q plasmids (H). After 12 hours, the supernatant was
1023 collected to purify ORF8 protein. After PNGase F digestion, the ORF8 protein was
1024 used to stimulate THP-1 DM cells. After 12 hours, the interaction of ORF8 and
1025 IL17RA was detected by co-immunoprecipitation. Representative images from n = 3
1026 biological replicates are shown.

1027 (I, J) Brefeldin A (3 µg/mL) or Monensin (2 µM) was used to pretreat Calu-3 cells for
1028 2 hours, followed by infection with SARS-CoV-2 ORF8-N78Q variant (I), or
1029 transfection with ORF8-N78Q plasmids (J). Twelve hours later, the supernatant was
1030 used to stimulate THP-1 DM cells for another 12 hours. The interaction of ORF8 and

1031 IL17RA was detected by co-immunoprecipitation. Representative images from n = 3
1032 biological replicates are shown.
1033 One-way ANOVA followed by Bonferroni post *hoc* test (D, E) was used for data
1034 analysis. *, p < 0.05, **, p < 0.01.

1035

1036 **Figure 5 N-linked glycosylation of ORF8 protects mice from cytokine storm**
1037 (A, B) Synthetic N-linked-glycosylated ORF8 (ORF8-N-Glyc) (1 μ g/mL) was added
1038 into the cell culture medium of THP-1 DM cells to stimulate IL-17 pathway. The
1039 interaction of ORF8 and IL17RA was detected by co-immunoprecipitation (A). The
1040 release of cytokines and chemokines was detected by ELISA (B). Representative
1041 images from n = 3 biological replicates are shown (A). Data are shown as the mean \pm
1042 s.e.m. of n = 3 biological replicates (B).
1043 (C) Survival of K18-hACE2 mice infected with PBS (n = 11), unglycosylated ORF8
1044 (n = 18) or synthetic N-linked-glycosylated ORF8 proteins (n = 17) (200 μ g/mouse).
1045 Data are shown as Kaplan-Meier curves.
1046 (D) Lung lesions of K18-hACE2 mice infected with unglycosylated ORF8 or
1047 synthetic N-linked-glycosylated ORF8 proteins (200 μ g/mouse) were detected by
1048 H&E staining at day 7 post infection (dpi). Representative images from n = 6
1049 biological replicates are shown. Scale bar = 500 μ m.
1050 (E, F) The release of cytokines and chemokines in lungs (E) and livers (F), which
1051 were obtained from K18-hACE2 mice intranasally infected with unglycosylated
1052 ORF8 or synthetic N-linked-glycosylated ORF8 proteins (200 μ g/mouse), was

1053 detected by ELISA at 7 dpi. Data are shown as the mean \pm s.e.m. of n = 6 biological
1054 replicates.

1055 Log-rank (Mantel-Cox) test (C) and one-way ANOVA followed by Bonferroni post
1056 *hoc* test (B, E, F) were used for data analysis. *, p < 0.05, **, p < 0.01.

1057

1058 **Figure 6 YIF1B interacts with unconventionally secreted ORF8**

1059 (A) Flag-tagged ORF8 was transfected into HEK-293FT cells. After 12 hours, the
1060 interaction of ORF8 and endogenic YIF1B was detected by co-immunoprecipitation.
1061 Representative images from n = 3 biological replicates are shown.

1062 (B, C) Flag-tagged ORF8 and HA-tagged YIF1B were co-transfected into
1063 HEK-293FT cells. After 12 hours, the interaction of ORF8 and YIF1B was detected
1064 by co-immunoprecipitation (B) and Duolink PLA assay (C). Representative images
1065 from n = 3 biological replicates are shown.

1066 (D) Calu-3 cells were infected with SARS-CoV-2 for 12 hours at a dosage of 10^5
1067 TCID₅₀/mL. The interaction of ORF8 and YIF1B was detected by
1068 co-immunoprecipitation. Representative images from n = 3 biological replicates are
1069 shown. Scale bar = 10 μ m.

1070 (E, F) Wild-type and YIF1B-KO cells were transfected with HA-tagged YIF1B,
1071 followed by infection with SARS-CoV-2 for 12 hours at a dosage of 10^5 TCID₅₀/mL.
1072 The secretion of ORF8 was detected by western blotting (E) and ELISA (F). Brefeldin
1073 A (3 μ g/mL) was used to block conventional secretion of ORF8. Representative
1074 images from n = 3 biological replicates are shown (E). Data are shown as the mean \pm

1075 s.e.m. of n = 3 biological replicates (F).

1076 (G) Wild-type and YIF1B-KO cells were transfected with HA-tagged YIF1B, and
1077 were infected with SARS-CoV-2 for 12 hours at a dosage of 10^5 TCID₅₀/mL. The cell
1078 culture supernatant was collected to stimulate THP-1 DM cells for 12 hours. The
1079 release of cytokines and chemokines was detected by ELISA. Data are shown as the
1080 mean \pm s.e.m. of n = 3 biological replicates.

1081 (H, I) Wild-type and YIF1B-KO cells were co-transfected with Flag-tagged ORF8 and
1082 HA-tagged YIF1B. After 12 hours, the secretion of ORF8 was detected by western
1083 blotting (H) and ELISA (I). Brefeldin A (3 μ g/mL) was used to block conventional
1084 secretion of ORF8. Representative images from n = 3 biological replicates are shown
1085 (H). Data are shown as the mean \pm s.e.m. of n = 3 biological replicates (I).

1086 (J) Wild-type and YIF1B-KO cells were co-transfected with Flag-tagged ORF8 and
1087 HA-tagged YIF1B. Twelve hours later, the cell culture supernatant was collected to
1088 stimulate THP-1 DM cells for another 12 hours. The release of cytokines and
1089 chemokines was detected by ELISA. Data are shown as the mean \pm s.e.m. of n = 3
1090 biological replicates.

1091 Unpaired two-tailed Student *t* test (F, I) and one-way ANOVA followed by Bonferroni
1092 post *hoc* test (G, J) were used for data analysis. *, p < 0.05, **, p < 0.01.

1093

1094

1095 **Figure 7 β 8 sheet of ORF8 and α 4 helix of YIF1B are essential for the interaction**

1096 (A) Structure of β -pleated sheet in SARS-CoV-2 ORF8 protein.

1097 (B) ORF8 β sheet mutants ($\Delta\beta 1$ - $\Delta\beta 8$) were transfected into Calu-3 cells. After 12
1098 hours, the interaction of ORF8 and YIF1B was detected by co-immunoprecipitation.
1099 Representative images from $n = 3$ biological replicates are shown.
1100 (C, D) ORF8 β sheet mutants ($\Delta\beta 1$ - $\Delta\beta 8$) were transfected into Calu-3 cells. After 12
1101 hours, the secretion of ORF8 was detected by western blotting (C) and ELISA (D).
1102 Brefeldin A (3 $\mu\text{g/mL}$) was used to block conventional secretion of ORF8.
1103 Representative images from $n = 3$ biological replicates are shown (C). Data are shown
1104 as the mean \pm s.e.m. of $n = 3$ biological replicates (D).
1105 (E) ORF8 $\Delta\beta 8$ mutant was transfected into Calu-3 cells. Twelve hours later, the cell
1106 culture supernatant was collected to stimulate THP-1 DM cells for another 12 hours.
1107 The release of cytokines and chemokines was detected by ELISA. Brefeldin A (3
1108 $\mu\text{g/mL}$) was used to block conventional secretion of ORF8. Data are shown as the
1109 mean \pm s.e.m. of $n = 3$ biological replicates.
1110 (F) Structure of α helix and corresponding deletion mutants of YIF1B protein.
1111 (G) YIF1B α helix mutants ($\Delta\alpha 1$ - $\Delta\alpha 5$) were transfected into Calu-3 cells. After 12
1112 hours, the interaction of ORF8 and YIF1B was detected by co-immunoprecipitation.
1113 Representative images from $n = 3$ biological replicates are shown.
1114 (H, I) YIF1B α -helix mutants ($\Delta\alpha 1$ - $\Delta\alpha 5$) were transfected into wild-type Calu-3 cells.
1115 After 12 hours, the secretion of ORF8 was detected by western blotting (H) and
1116 ELISA (I). Brefeldin A (3 $\mu\text{g/mL}$) was used to block conventional secretion of ORF8.
1117 Representative images from $n = 3$ biological replicates are shown (H). Data are shown
1118 as the mean \pm s.e.m. of $n = 3$ biological replicates (I).

1119 (J) YIF1B $\Delta\alpha 4$ mutant was transfected into wild-type Calu-3 cells. Twelve hours later,
1120 the cell culture supernatant was collected to stimulate THP-1 DM cells for another 12
1121 hours. The release of cytokines and chemokines was detected by ELISA. Brefeldin A
1122 (3 μ g/mL) was used to block conventional secretion of ORF8. Data are shown as the
1123 mean \pm s.e.m. of n = 3 biological replicates.

1124 (K, L) YIF1B α -helix mutants ($\Delta\alpha 1$ - $\Delta\alpha 5$) were transfected into YIF1B-KO Calu-3
1125 cells. After 12 hours, the secretion of ORF8 was detected by western blotting (K) and
1126 ELISA (L). Brefeldin A (3 μ g/mL) was used to block conventional secretion of ORF8.
1127 Representative images from n = 3 biological replicates are shown (K). Data are shown
1128 as the mean \pm s.e.m. of n = 3 biological replicates (L).

1129 (M) YIF1B $\Delta\alpha 4$ mutant was transfected into YIF1B-KO Calu-3 cells. The cell culture
1130 supernatant was collected to stimulate THP-1 DM cells for 12 hours. The release of
1131 cytokines and chemokines was detected by ELISA. Brefeldin A (3 μ g/mL) was used
1132 to block conventional secretion of ORF8. Data are shown as the mean \pm s.e.m. of n =
1133 3 biological replicates.

1134 (N, O) HA-tagged YIF1B, V5-tagged 3CL pro and V5-tagged 3CL pro containing $\beta 8$
1135 sheet were transfected into YIF1B-KO Calu-3 cells. After 12 hours later, the
1136 interaction of YIF1B and 3CL pro was detected by co-immunoprecipitation (N). The
1137 secretion of 3CL pro was detected by western blotting (O). Representative images
1138 from n = 3 biological replicates are shown.

1139 One-way ANOVA followed by Bonferroni post *hoc* test (E, I, J, L, M) was used for
1140 data analysis. *, p < 0.05, **, p < 0.01. Abbreviations: n.s., not significant.

1141

1142

1143 **Figure 8 YIF1B promotes the transport of ORF8**

1144 (A) Calu-3 cells were infected with SARS-CoV-2, or transfected with ORF8-Flag.

1145 After 12 hours, the co-localization of ORF8 and YIF1B was observed by

1146 immunofluorescence. Representative images from n = 3 biological replicates are

1147 shown. Scale bar = 10 μ m.

1148 (B) Calu-3 cells were transfected with ORF8- $\Delta\beta8$ mutant. After 12 hours, the

1149 co-localization of ORF8 and YIF1B was observed by immunofluorescence.

1150 Representative images from n = 3 biological replicates are shown. Scale bar = 10 μ m.

1151 (C) Calu-3 cells were infected with SARS-CoV-2, or transfected with ORF8-Flag.

1152 YIF1B- $\Delta\alpha4$ mutant was also transfected into Calu-3 cells. After 12 hours, the

1153 co-localization of ORF8 and YIF1B was observed by immunofluorescence.

1154 Representative images from n = 3 biological replicates are shown. Scale bar = 10 μ m.

1155 (D) ORF8 and YIF1B α -helix mutants ($\Delta\alpha1-\Delta\alpha5$) were transfected into YIF1B-KO

1156 Calu-3 cells. Whole cell lysates were collected for Proteinase K protection assay. PDI

1157 and SEC22B were used as positive control and negative control, respectively.

1158 Representative images from n = 3 biological replicates are shown.

1159 (E, F) Schematic diagram of *in vitro* translocation assay (E). Different doses of YIF1B

1160 protein and lipids were assembled to proteoliposomes. ORF8 protein and synthetic

1161 proteoliposomes were mixed in the lysate of HEK-293FT cells (without

1162 endomembrane). Proteoliposomes containing ORF8 were collected and aliquoted into

1163 three parts for Proteinase K protection assay (F). Representative images from n = 3
1164 biological replicates are shown (F).

1165 (G) Schematic diagram of GFP fluorescence complementation system. ORF8 fused
1166 with GFP (11) and YIF1B containing GFP (1-10), were co-transfected into
1167 HEK-293FT cells, and flow cytometry was used to measure GFP fluorescence
1168 intensity.

1169 (H, I) Different doses of ORF8-GFP(11) were co-transfected with YIF1B-GFP(1-10)
1170 (H), or different doses of YIF1B-GFP(1-10) (I) were co-transfected with
1171 ORF8-GFP(11) into HEK-293FT cells, and flow cytometry was used to measure GFP
1172 fluorescence intensity. Representative images from n = 3 biological replicates are
1173 shown. Data are shown as the mean \pm s.e.m. of n = 3 biological replicates.

1174 One-way ANOVA followed by Bonferroni post *hoc* test (H, I) was used for data
1175 analysis. *, p < 0.05. Abbreviations: n.s., not significant.

1176

1177

1178 **Figure 9 YIF1B-deficient mice resist to SARS-CoV-2-induced cytokine storm**
1179 (A) AECs obtained from *Yif1b*^{-/-} mice and their littermates (*Yif1b*^{+/+}) were infected
1180 with SARS-CoV-2 for 12 hours at a dosage of 10⁵ TCID₅₀/mL. The interaction of
1181 ORF8 and YIF1B was detected by co-immunoprecipitation (A). HA-tagged YIF1B
1182 was transfected into cells to restore YIF1B expression. The secretion of ORF8 was
1183 detected by ELISA (B). Representative images from n = 3 biological replicates are
1184 shown (A). Data are shown as the mean \pm s.e.m. of n = 3 biological replicates (B).

1185 (C) AECs obtained from *Yif1b*^{-/-} mice and their littermates (*Yif1b*^{+/+}) were infected
1186 with SARS-CoV-2, or transfected with ORF8-Flag plasmids. After 12 hours, the
1187 supernatant was collected to purify ORF8 protein. After PNGase F digestion, ORF8
1188 protein was detected by western blotting. Representative images from n = 3 biological
1189 replicates are shown.

1190 (D, E) AECs obtained from *Yif1b*^{-/-} mice and their littermates (*Yif1b*^{+/+}) were infected
1191 with SARS-CoV-2 at a dosage of 10⁵ TCID₅₀/mL. After 12 hours, the supernatant was
1192 collected to purify ORF8 protein, which was used to stimulate THP-1 DM cells for
1193 another 12 hours. The interaction of ORF8 and IL17RA was detected by
1194 co-immunoprecipitation (D). The activation of IL-17 pathway was evaluated by
1195 testing NF-κB activity (E). Representative images from n = 3 biological replicates are
1196 shown (D). Data are shown as the mean ± s.e.m. of n = 3 biological replicates (E).

1197 (F) Survival of *Yif1b*^{-/-} mice (n = 16) and their littermates (*Yif1b*^{+/+}, n = 14) after
1198 intranasal infection with SARS-CoV-2 with 4×10⁵ PFU. Data are shown as
1199 Kaplan-Meier curves.

1200 (G) Lung lesions of *Yif1b*^{-/-} mice and their littermates (*Yif1b*^{+/+}) were detected by H&E
1201 staining at 7 dpi. Representative images from n = 6 biological replicates are shown.
1202 Scale bar = 500 μm.

1203 (H) Viral loads in lungs obtained from *Yif1b*^{-/-} mice and their littermates (*Yif1b*^{+/+}) at 7
1204 dpi. Data are shown as the mean ± s.e.m. of n = 6 biological replicates.
1205 (I, J) The secretion of cytokines and chemokines in lungs (I) and livers (J) obtained
1206 from *Yif1b*^{-/-} mice and their littermates (*Yif1b*^{+/+}) at 7 dpi, was detected by ELISA.

1207 Data are shown as the mean \pm s.e.m. of $n = 6$ biological replicates.

1208 Two-way ANOVA followed by Bonferroni post *hoc* test (B, E, I, J), Log-rank

1209 (Mantel-Cox) test (F) and unpaired two-tailed Student *t* test (H) were used for data

1210 analysis. *, $p < 0.05$, **, $p < 0.01$. Abbreviations: n.s., not significant.

1211

1212 **Figure 10 Schematic representation of conventional and unconventional secretion**
1213 **of ORF8 during SARS-CoV-2 infection**

1214

1215 **Figure S1 SARS-CoV-2 ORF8 can be secreted without the presence of complete**
1216 **virus**

1217 (A) Validation of Calu-3 *Ace2*^{+/+}, Calu-3 *Ace2*^{-/-}, THP-1 DM *Il17ra*^{+/+} and THP-1 DM
1218 *Il17ra*^{-/-} cells. The expressions of ACE2 and IL17RA were detected by western
1219 blotting. Representative images from $n = 3$ biological replicates are shown.

1220 (B) Schematic diagram of THP-1 DM cells stimulation model. HEK-293FT cells were
1221 transfected with Flag-tagged ORF8, 3CL pro, or Nef. After 12 hours, the supernatant
1222 was collected and divided into two parts. One part was used to purify secretory
1223 proteins, followed by western blotting; the other part was used to stimulate THP-1
1224 DM cells for 12 hours. The release of cytokines and chemokines was detected by
1225 ELISA.

1226 (C) Secretory proteins obtained from HEK-293FT cell supernatant in (B) were
1227 detected by western blotting. Representative images from $n = 3$ biological replicates
1228 are shown.

1229 (D) The release of cytokines and chemokines from THP-1 DM cells in (B) was
1230 detected by ELISA. Data are shown as the mean \pm s.e.m. of n = 3 biological
1231 replicates.

1232 One-way ANOVA followed by Bonferroni post *hoc* test (D) was used for data analysis.

1233 *, p < 0.05, **, p < 0.01.

1234

1235 **Figure S2 SARS ORF8a cannot be glycosylated**

1236 (A, B) Brefeldin A (3 μ g/mL) or Monensin (2 μ M) was used to pretreat Calu-3 cells
1237 for 2 hours, followed by SARS-CoV-2 infection for 12 hours at a dosage of 10^5
1238 TCID₅₀/mL (A), or Flag-tagged ORF8 plasmid transfection for 12 hours (B). The
1239 supernatant was collected to stimulate THP-1 DM cells within the specified time. The
1240 release of cytokines and chemokines was detected by ELISA. Data are shown as the
1241 mean \pm s.e.m. of n = 3 biological replicates.

1242 (C) PNGase F (1,000 units/ μ g protein), O-Glycosidase (4,000 units/ μ g protein) or
1243 α 2-3, 6, 8, 9 Neuraminidase A (4 units/ μ g glycoprotein) was added into purified
1244 SARS ORF8a protein to release glycans. Western blotting was used to detect the
1245 glycosylation of ORF8a protein. Representative images from n = 3 biological
1246 replicates are shown.

1247 (D) Calu-3 cells were transfected with SARS ORF8a-Flag plasmids. Tunicamycin (2
1248 μ g/mL) was added into Calu-3 cells for 2 hours to prevent N-linked glycosylation, or
1249 PNGase F (1,000 units/ μ g protein) was used to remove the N-linked glycosylation in
1250 purified ORF8 protein. After deglycosylation assays, the cell culture supernatant or

1251 purified ORF8a protein was used to stimulate THP-1 DM cells. After 12 hours, the
1252 release of cytokines and chemokines was detected by ELISA. Data are shown as the
1253 mean \pm s.e.m. of n = 3 biological replicates.

1254 Two-way (A, B) or one-way (D) ANOVA followed by Bonferroni post *hoc* test was
1255 used for data analysis. Abbreviations: n.s., not significant.

1256

1257 **Figure S3 ORF8 N78 glycosylation blocks the activation of IL-17 pathway**

1258 (A) Calu-3 cells were infected with SARS-CoV-2 ORF8-N78Q variant, or transfected
1259 with ORF8-N78Q plasmids. Twelve hours later, the supernatant was used to stimulate
1260 THP-1 DM cells for another 12 hours. The activation of IL-17 pathway was evaluated
1261 by testing NF- κ B activity. Data are shown as the mean \pm s.e.m. of n = 3 biological
1262 replicates.

1263 (B, C) Calu-3 cells were infected with SARS-CoV-2 ORF8-N78Q variant (B), or
1264 transfected with ORF8-N78Q plasmids (C). The supernatant was collected to purify
1265 ORF8 protein. After PNGase F digestion, the ORF8 protein was used to stimulate
1266 THP-1 DM cells. After 12 hours, the activation of IL-17 pathway was evaluated by
1267 testing NF- κ B activity. Data are shown as the mean \pm s.e.m. of n = 3 biological
1268 replicates.

1269 (D, E) Brefeldin A (3 μ g/mL) or Monensin (2 μ M) was used to pretreat Calu-3 cells
1270 for 2 hours, followed by infection with SARS-CoV-2 ORF8-N78Q variant (D) or
1271 transfection with ORF8-N78Q plasmids (E) for 12 hours. The supernatant was used to
1272 stimulate THP-1 DM cells for 12 hours. The secretion of ORF8 was detected by

1273 ELISA. Data are shown as the mean \pm s.e.m. of n = 3 biological replicates.

1274 (F, G) The activation of IL-17 pathway in (D, E) was evaluated by testing NF- κ B

1275 activity. Data are shown as the mean \pm s.e.m. of n = 3 biological replicates.

1276 Two-way ANOVA followed by Bonferroni post *hoc* test was used for data analysis. *,

1277 p < 0.05, **, p < 0.01. Abbreviations: n.s., not significant.

1278

1279 **Figure S4 SARS-CoV-2 ORF8 can be secreted through an unconventional**

1280 **pathway**

1281 (A) Calu-3 cells were infected with SARS-CoV-2 for 12 hours at a dosage of 10^5

1282 TCID₅₀/mL. Starvation assay (12 hours) or Rapamycin (50 nM) was used to induce

1283 autophagy. The secretion of ORF8 was detected by western blotting. Brefeldin A (3

1284 μ g/mL) was used to block conventional secretion of ORF8. Representative images

1285 from n = 3 biological replicates are shown.

1286 (B) Calu-3 cells were infected with SARS-CoV-2 for 12 hours at a dosage of 10^5

1287 TCID₅₀/mL. 3-MA (10 mM) or Wtm (20 nM) was used to inhibit the autophagy

1288 induced by starvation. The secretion of ORF8 was detected by western blotting.

1289 Brefeldin A (3 μ g/mL) was used to block conventional secretion of ORF8.

1290 Representative images from n = 3 biological replicates are shown.

1291 (C) Calu-3 cells were infected with SARS-CoV-2 for 12 hours at a dosage of 10^5

1292 TCID₅₀/mL. siRNA of *Atg5*, *Atg2a*, or *Atg2b* was transfected into cells to inhibit the

1293 autophagy induced by starvation. The secretion of ORF8 was detected by western

1294 blotting. Brefeldin A (3 μ g/mL) was used to block conventional secretion of ORF8.

1295 Representative images from n = 3 biological replicates are shown.

1296 (D) Calu-3 cells were infected with SARS-CoV-2, or transfected with ORF8-Flag.

1297 After 12 hours, the co-localization of ORF8 and ERGIC-53 was observed by

1298 immunofluorescence. Brefeldin A (3 μ g/mL) was used to block conventional secretion

1299 of ORF8. Representative images from n = 3 biological replicates are shown. Scale bar

1300 = 10 μ m.

1301 (E) Calu-3 cells were infected with SARS-CoV-2 for 12 hours at a dosage of 10^5

1302 TCID₅₀/mL. Whole cell lysates were collected for Proteinase K protection assay. PDI

1303 and SEC22B were used as positive control and negative control, respectively.

1304 Brefeldin A (3 μ g/mL) was used to block conventional secretion of ORF8.

1305 Representative images from n = 3 biological replicates are shown.

1306 (F) Schematic diagram of screening channel proteins secreted by ORF8 through an

1307 unconventional pattern. Brefeldin A (3 μ g/mL) or Monensin (2 μ M) was used to

1308 pretreat HEK-293FT cells for 2 hours, followed by transfection with

1309 DHFR/Flag-tagged ORF8 for 12 hours. Aminopterin was used to inhibit DHFR

1310 unfolding. Whole cell lysates were collected for HPLC-MS/MS analysis.

1311 Transmembrane proteins interacting with ORF8 both in Monensin and Brefeldin A

1312 treatment groups were considered as candidates.

1313 (G) Calu-3 cells were infected with SARS-CoV-2 for 12 hours at a dosage of 10^5

1314 TCID₅₀/mL. siRNAs of potential channel proteins were transfected into cells, and the

1315 secretion of ORF8 was detected by western blotting. Representative images from n =

1316 3 biological replicates are shown.

1317

1318 **Figure S5 Validation of *Yif1b*^{-/-} mice**

1319 (A) Schematic diagram of knockout strategy in generation of *Yif1b*^{-/-} hACE2 mice

1320 using CRISPR-Cas9. Two sgRNAs were designed to delete 3-5 exons of *Yif1b*.

1321 (B) PCR validation of *Yif1b*^{-/-} mice genotype. Representative images from n = 3

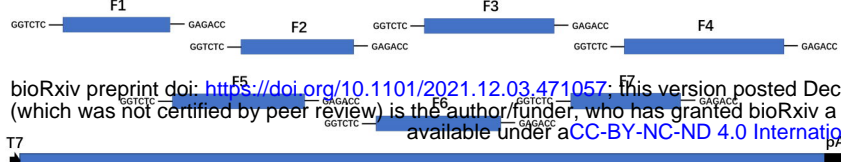
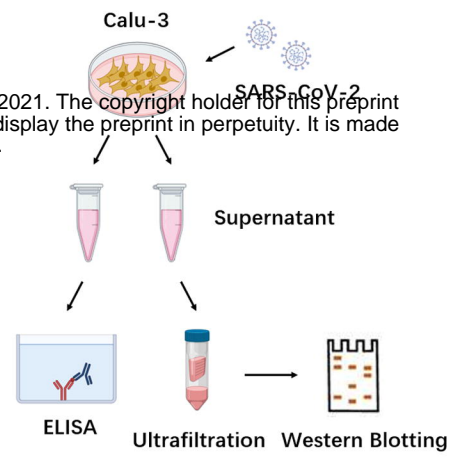
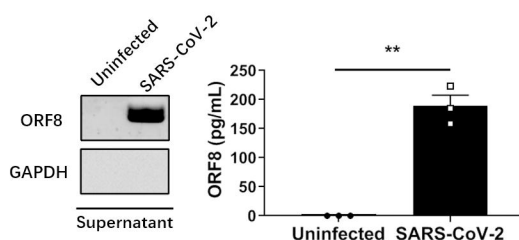
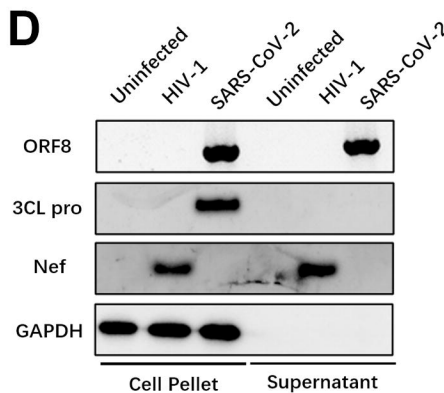
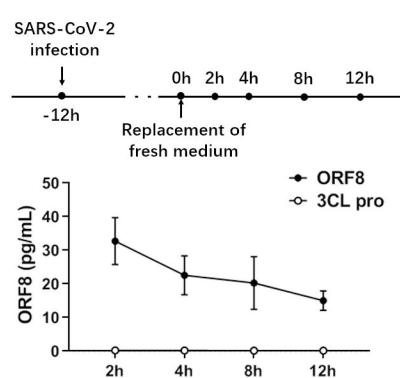
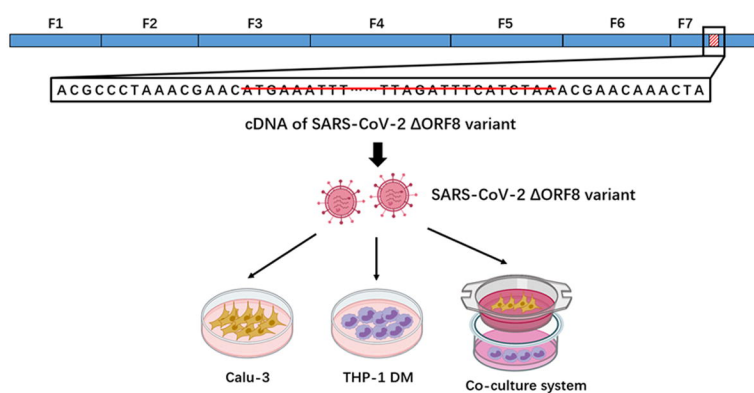
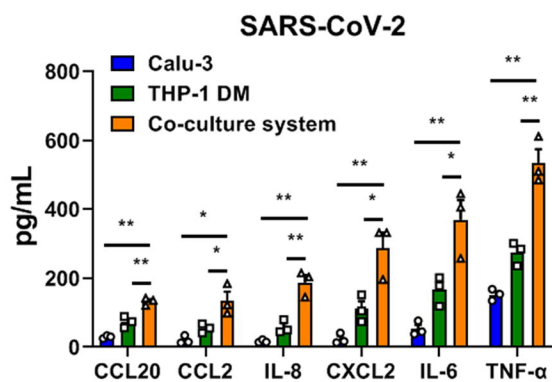
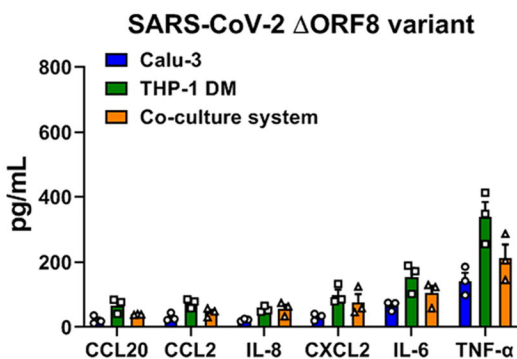
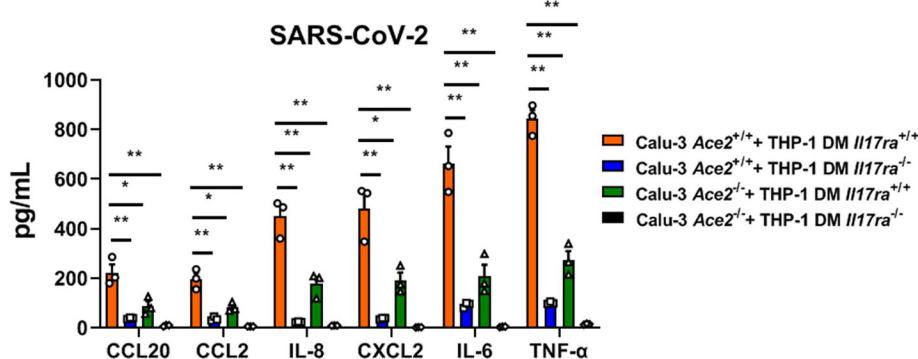
1322 biological replicates are shown.

1323 (C) The expressions of YIF1B in lungs obtained from *Yif1b*^{+/+} and *Yif1b*^{-/-} mice were

1324 detected by western blotting. Representative images from n = 3 biological replicates

1325 are shown.

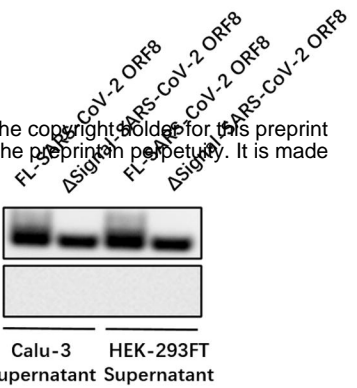
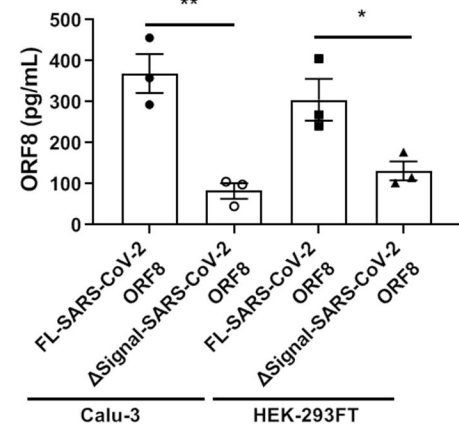
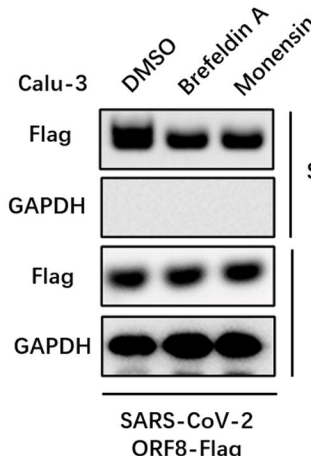
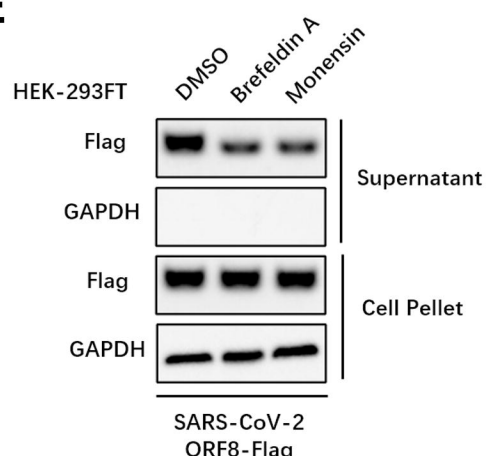
1326

A**B****C****D****E****F****G****H****I**

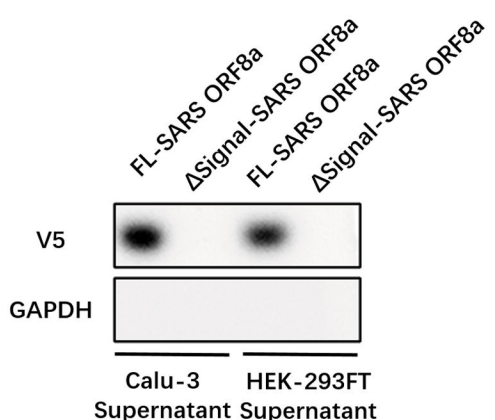
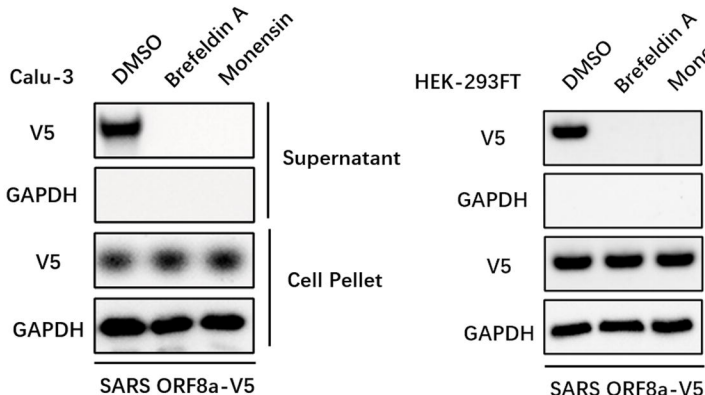
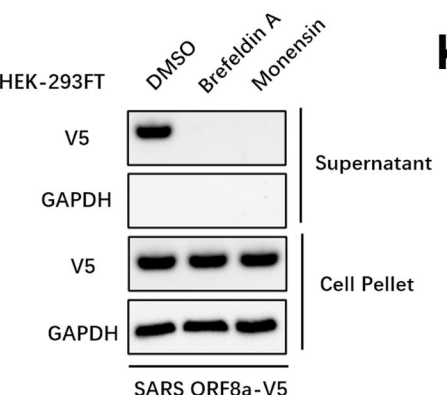
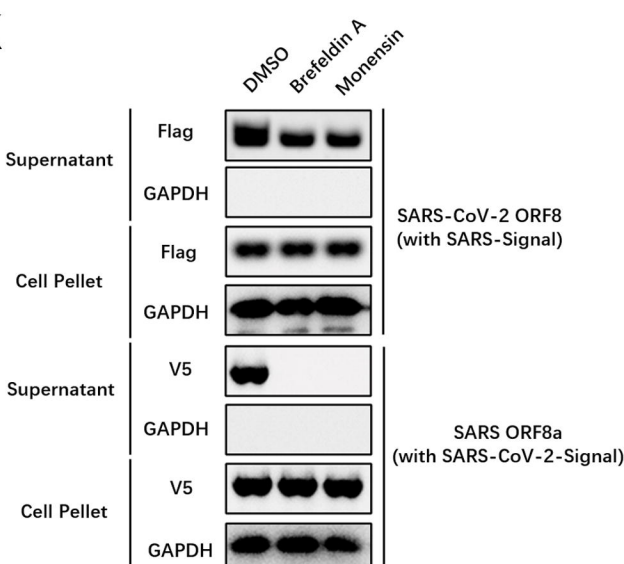
A

bioRxiv preprint doi: <https://doi.org/10.1101/2021.12.03.471057>; this version posted December 28, 2021. The copyright holder for this preprint (which was not certified by peer review) is the author/funder, who has granted bioRxiv a license to display the preprint in perpetuity. It is made available under aCC-BY-NC-ND 4.0 International license.

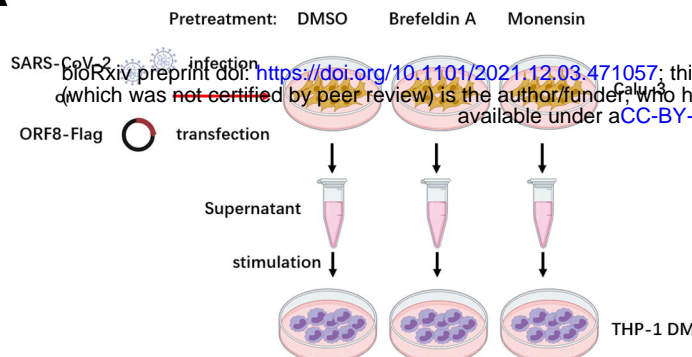
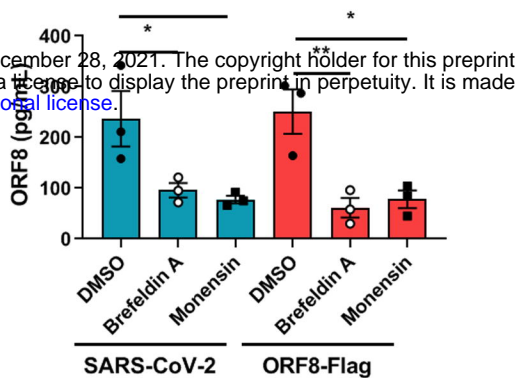
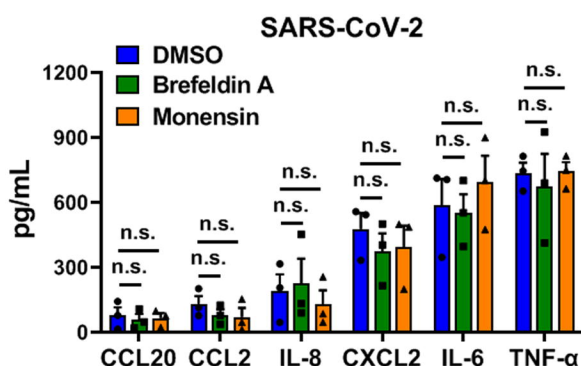
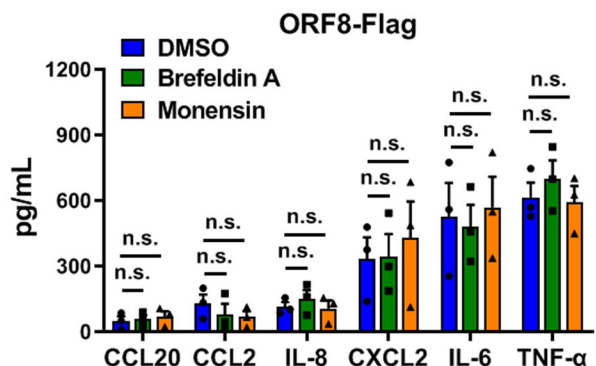
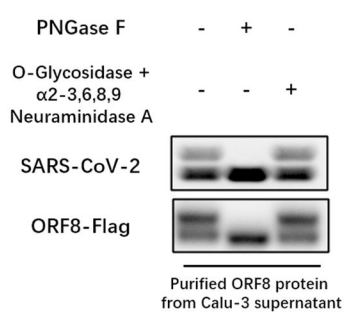
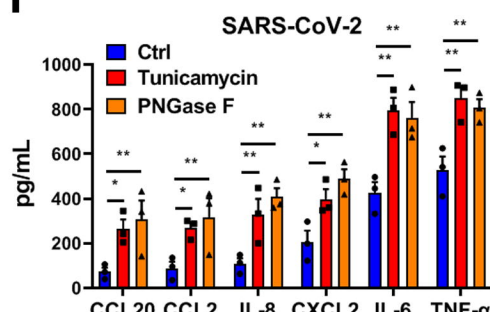
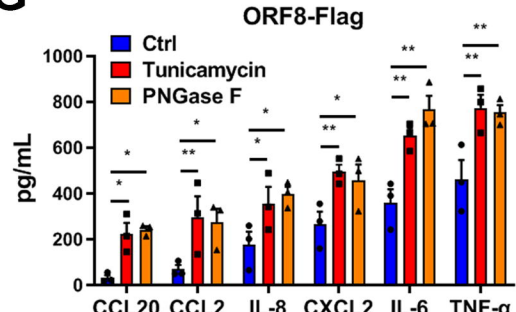
FL-SARS-CoV-2 ORF8 : M K F L V F L G I I T T V A A ——————Flag—————
 Δ Signal-SARS-CoV-2 ORF8 : [] ——————Flag—————

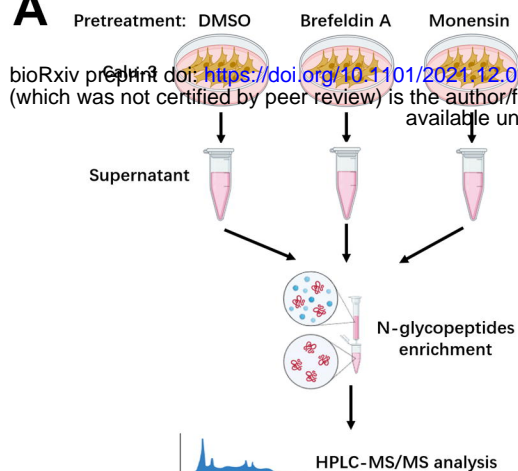
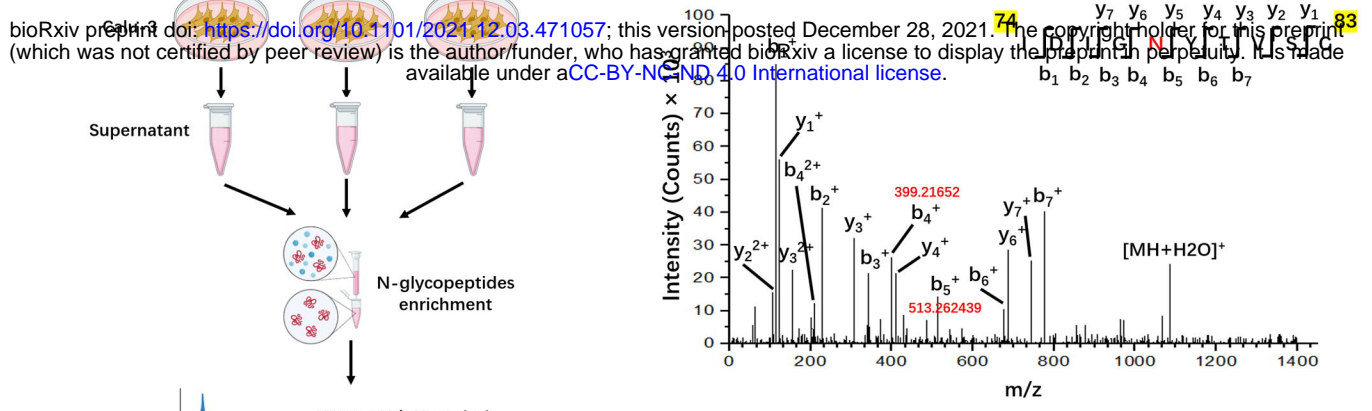
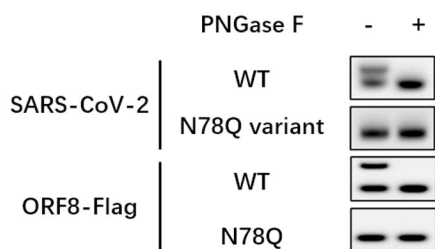
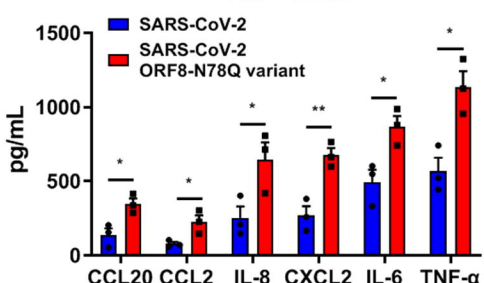
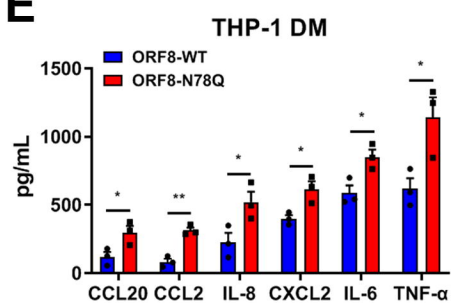
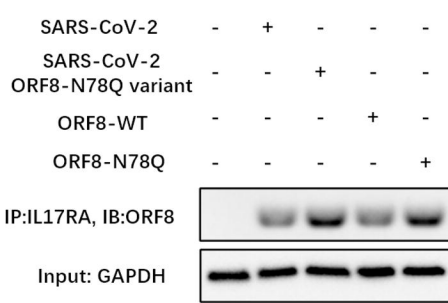
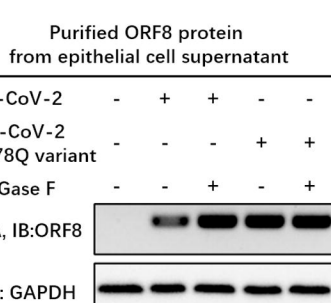
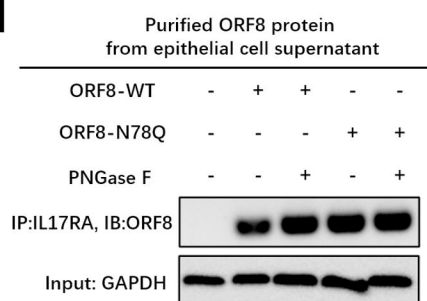
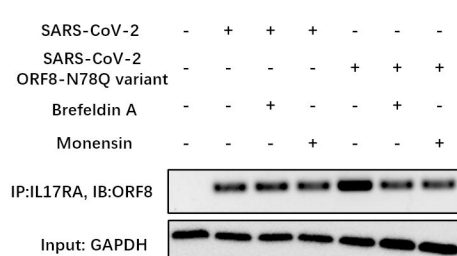
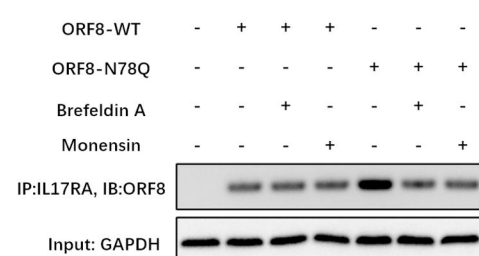
B**C****D****E****F**

FL-SARS ORF8a : M K L L I V L T C I S L C S C I C ——————V5—————
 Δ Signal-SARS ORF8a : [] ——————V5—————

G**H****I****K****J**

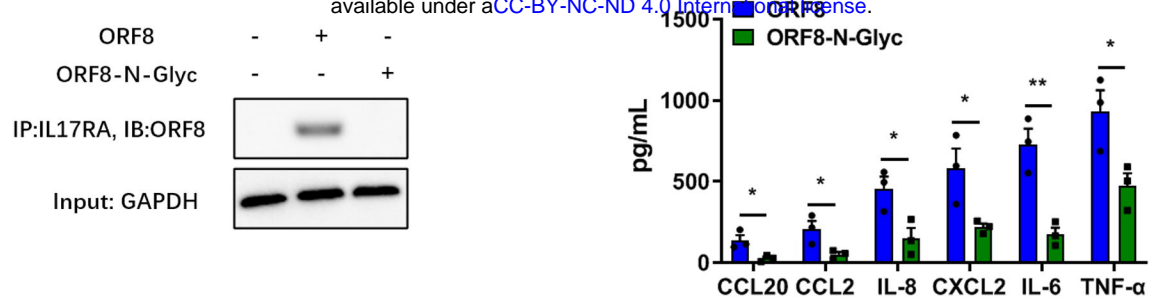
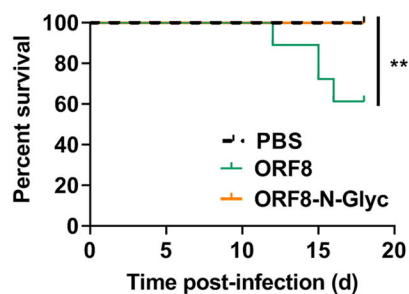
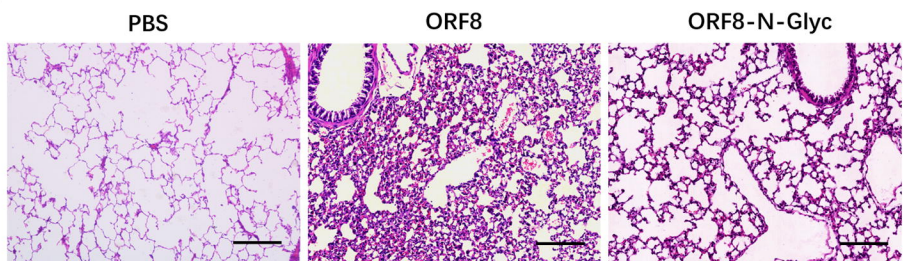
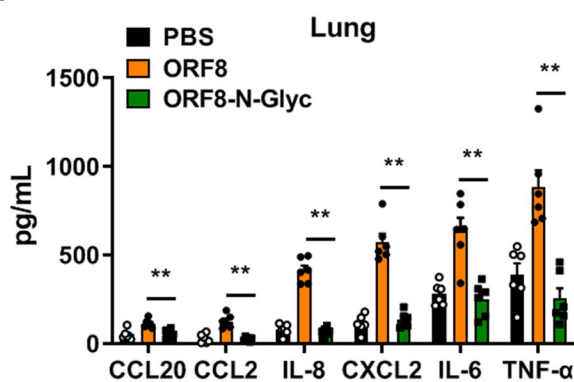
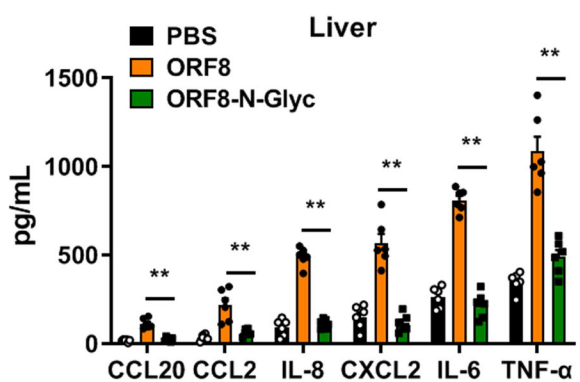
SARS-CoV-2 ORF8 (with SARS-Signal) : M K L L I V L T C I S L C S C I C ——————Flag—————
 SARS ORF8a (with SARS-CoV-2-Signal) : M K F L V F L G I I T T V A A ——————V5—————

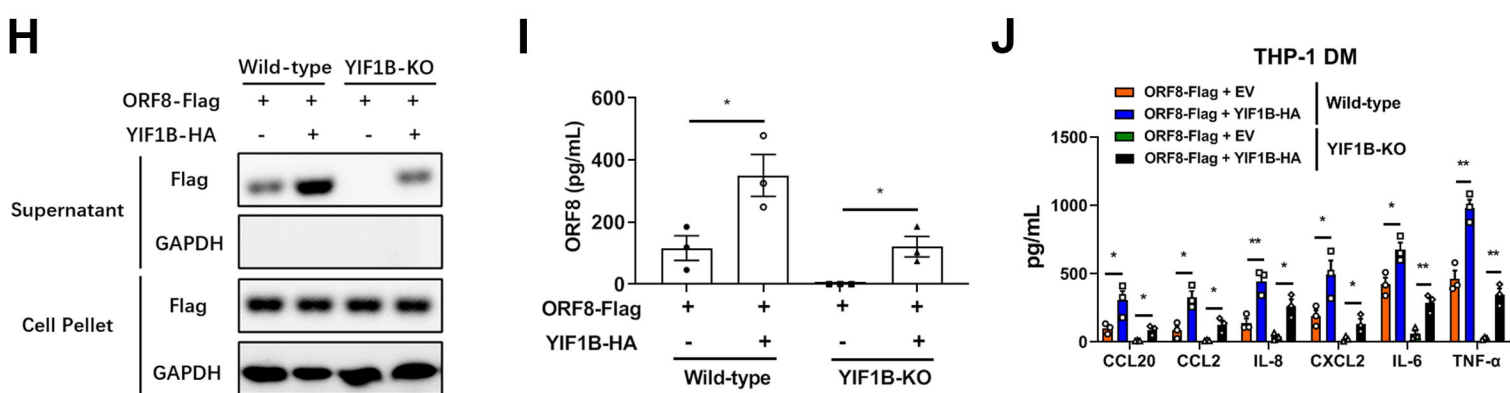
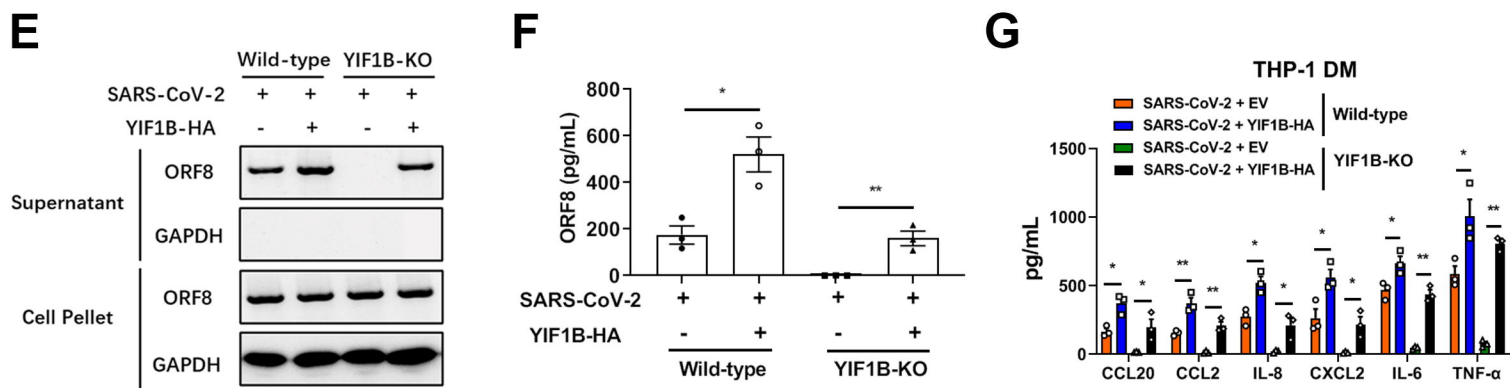
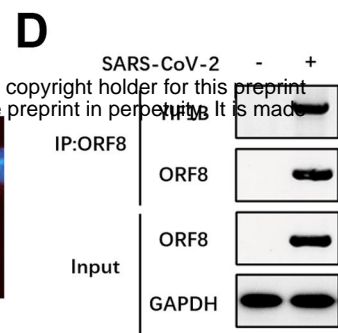
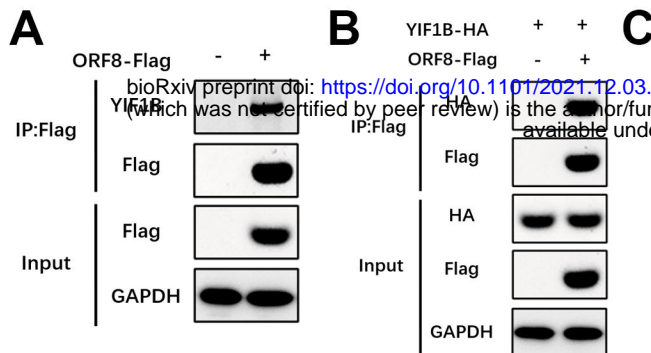
A**B****C****D****E****F****G**

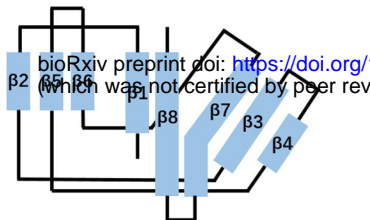
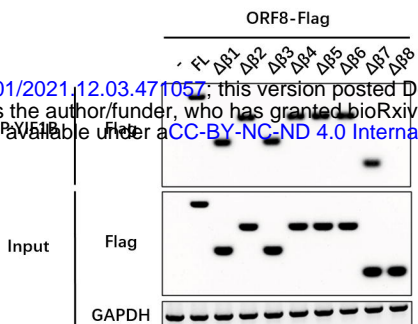
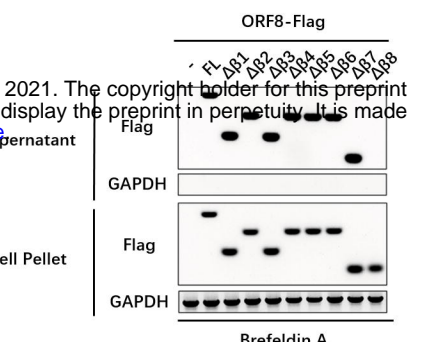
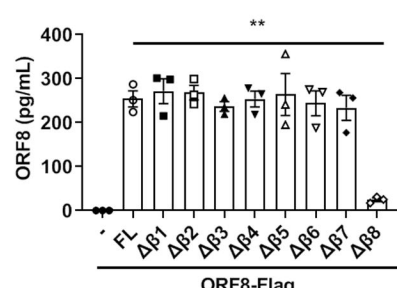
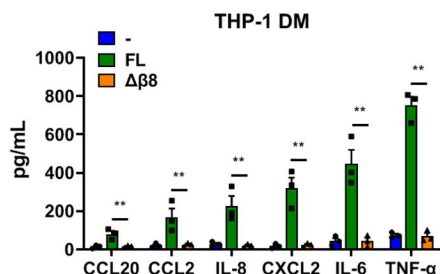
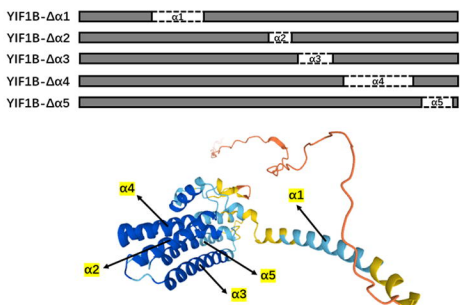
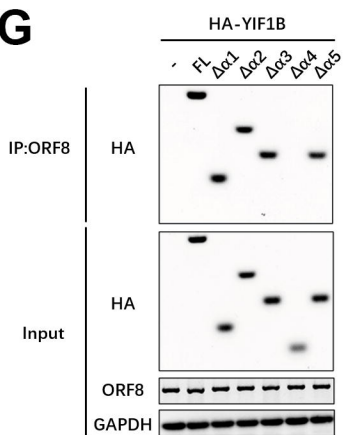
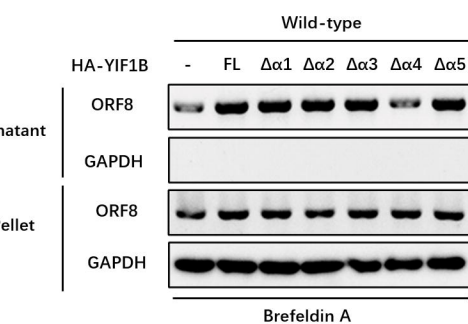
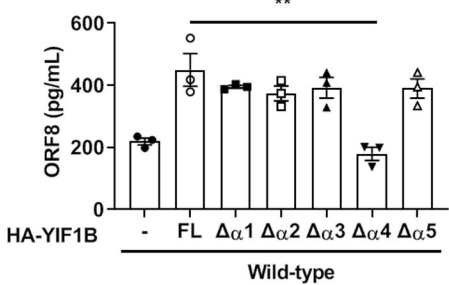
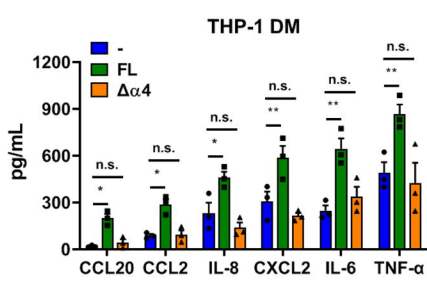
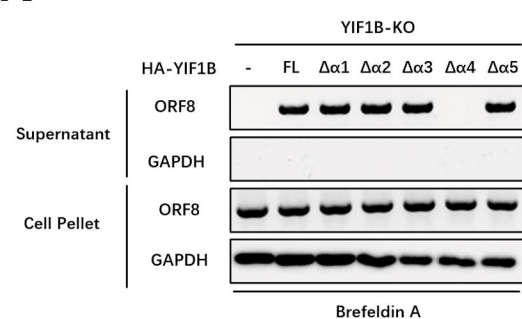
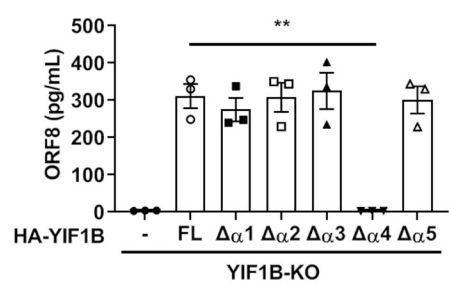
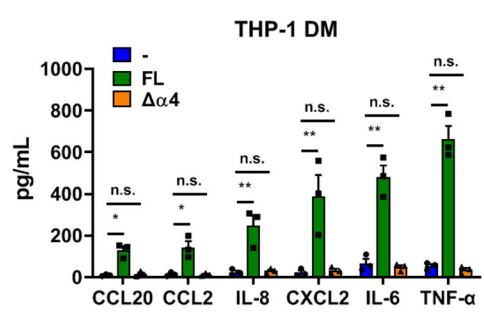
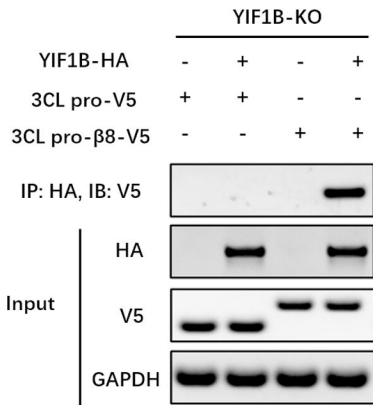
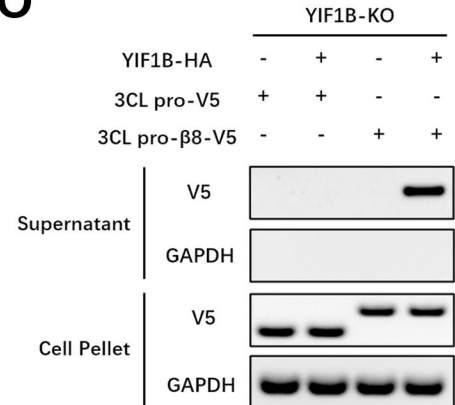
A**B****C****D****THP-1 DM****E****F****G****H****I****J**

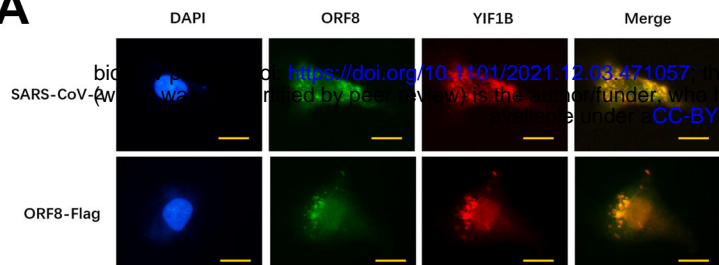
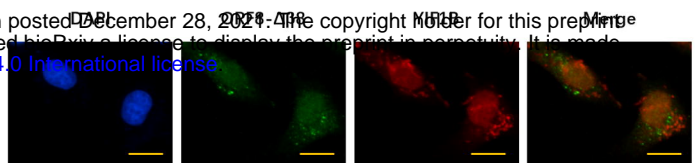
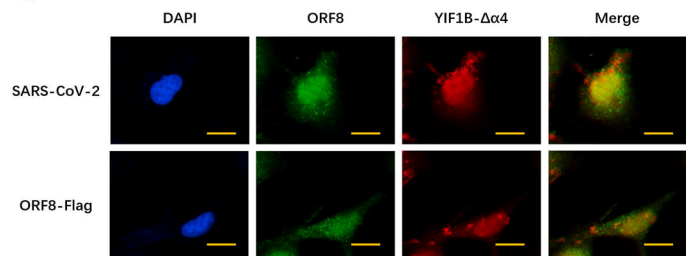
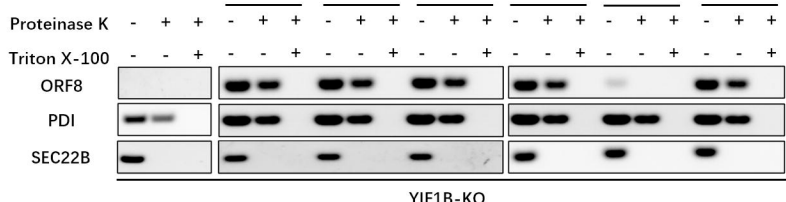
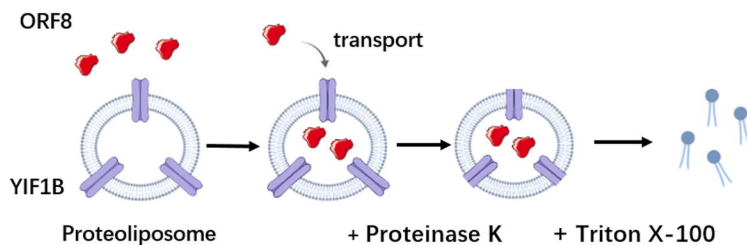
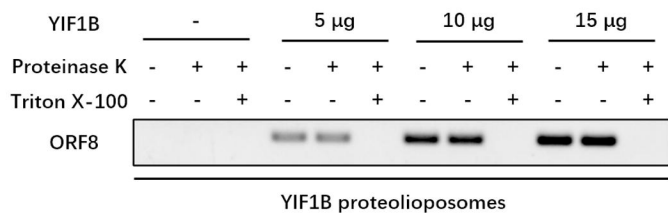
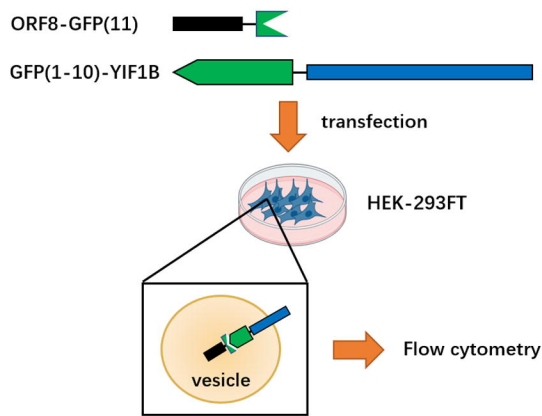
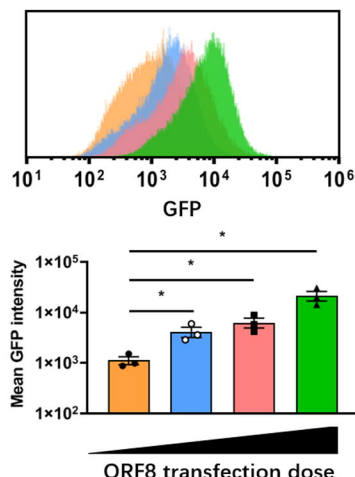
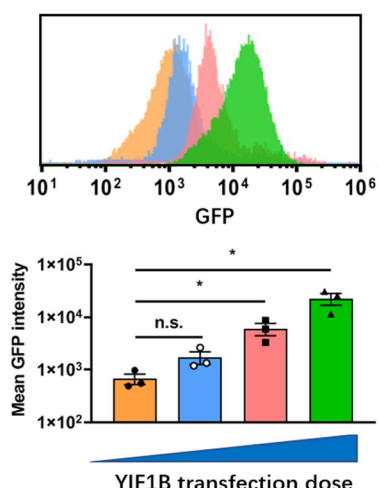
A

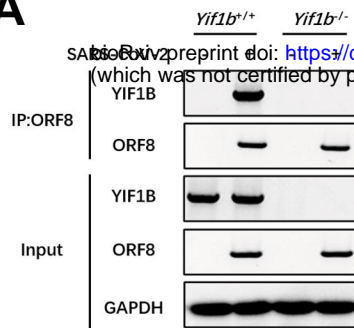
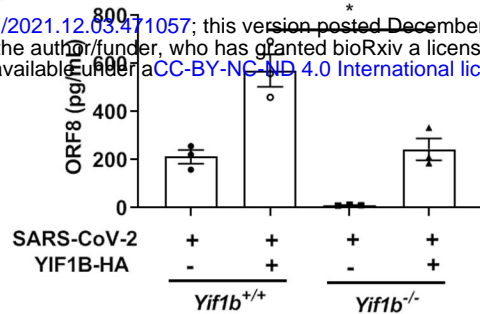
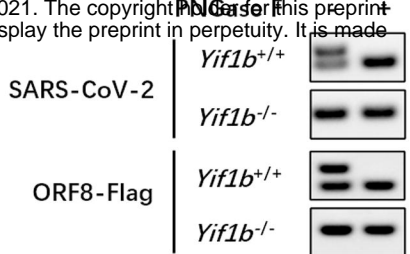
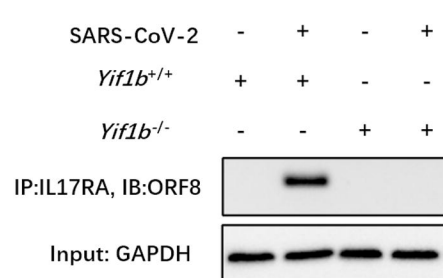
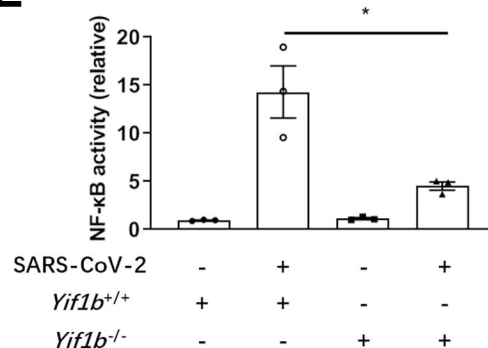
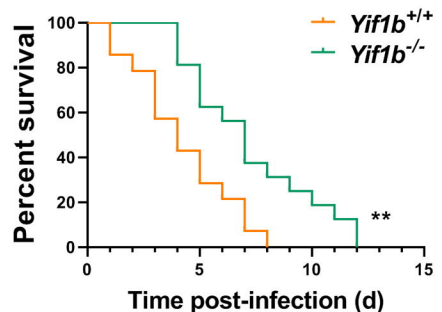
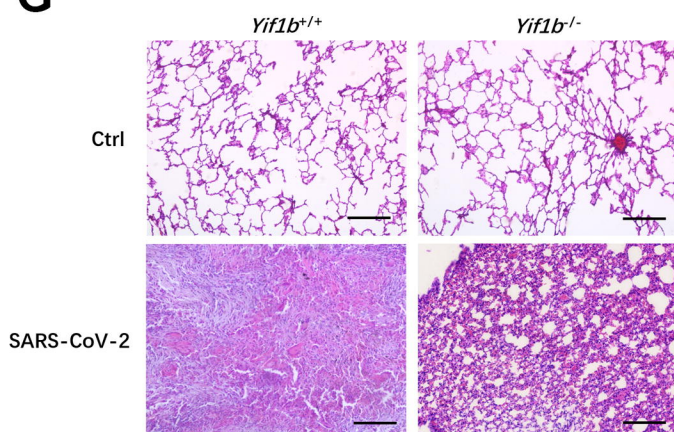
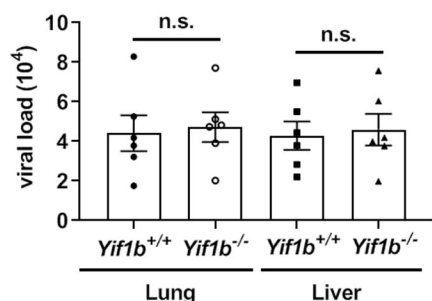
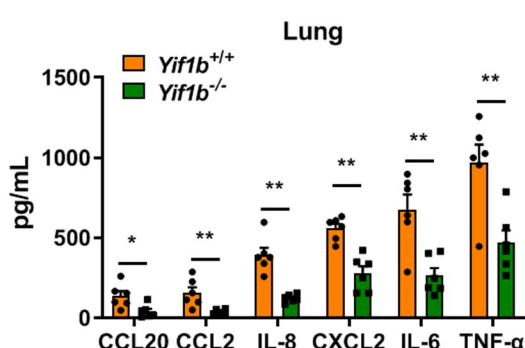
bioRxiv preprint doi: <https://doi.org/10.1101/2021.12.03.471057>; this version posted December 28, 2021. The copyright holder for this preprint (which was not certified by peer review) is the author/funder, who has granted bioRxiv a license to display the preprint in perpetuity. It is made available under aCC-BY-NC-ND 4.0 International license.

B**C****D****E****F**



A**B****C****D****E****F****G****H****I****J****K****L****M****N****O**

A**B****C****D****E****F****G****H****I**

A**B****C****D****E****F****G****H****I****J**